



Review

# Modeling Thermal Radiation in Combustion Environments: Progress and Challenges

Sandip Mazumder 1,\* and Somesh P. Roy 2 and Somesh P. Roy 2

- Department of Mechanical and Aerospace Engineering, The Ohio State University, Columbus, OH 43210, USA
- Department of Mechanical Engineering, Marquette University, Milwaukee, WI 53233, USA; somesh.roy@marquette.edu
- \* Correspondence: mazumder.2@osu.edu

Abstract: Modeling thermal radiation in combustion environments can be extremely challenging for two main reasons. First, the radiative transfer equation (RTE), which is the cornerstone of modeling radiation in such environments, is a five-dimensional integro-differential equation. Second, the absorption and scattering coefficients of molecular gases and particulates prevalent in combustion environments oscillate strongly with the wavenumber (or wavelength), i.e., the medium is strongly nongray, requiring the solution of the RTE for a large number of wavenumbers. This article reviews the progress that has been made in this area to date with an emphasis on the work performed over the past three decades. Progress in both deterministic and stochastic (Monte Carlo) solutions of the RTE is reviewed, in addition to the review of the treatment of the spectral properties of gases, soot, and fuel droplets that dominate combustion environments, i.e., spectral or nongray models. The application of the various state-of-the-art nongray models and RTE solution methods to flames (particularly turbulent), fires, combustors, and other combustion systems are summarized along with a critical discussion of the pros and cons of the models and methods. Finally, the challenges that remain in modeling thermal radiation in combustion systems are highlighted and future outlooks are shared.

Keywords: radiation; combustion; nongray; flame; TRI; RTE solver; Monte Carlo; FSK



Citation: Mazumder, S.; Roy, S.P. Modeling Thermal Radiation in Combustion Environments: Progress and Challenges. *Energies* **2023**, *16*, 4250. https://doi.org/10.3390/ en16104250

Academic Editor: Jian Liu

Received: 8 May 2023 Revised: 18 May 2023 Accepted: 19 May 2023 Published: 22 May 2023



Copyright: © 2023 by the authors. Licensee MDPI, Basel, Switzerland. This article is an open access article distributed under the terms and conditions of the Creative Commons Attribution (CC BY) license (https://creativecommons.org/licenses/by/4.0/).

### 1. Introduction

Thermal radiation is often the dominant mode of heat transfer in high-temperature combustion environments. Radiation transport in combustion environments is modeled using the radiative transfer equation (RTE). For typical (i.e., terrestrial) length scales in combustion applications, radiation transport is almost instantaneous, and it is sufficient to solve the steady-state RTE. The steady-state RTE is a five-dimensional integro-differential equation [1]: three spatial coordinates and two directional coordinates, making it challenging to solve. This difficulty is exacerbated by the fact that the absorption coefficient of molecular gases and particulates prevalent in combustion environments oscillates wildly with the wavelength (or wavenumber) [1,2], i.e., the medium is strongly nongray, which requires the solution of the RTE numerous times. With the advent of high-performance computing and increase in computational power, tremendous progress has been made in modeling radiation in combustion systems since the start of the current millennium. These advances have been summarized in several recent review articles and texts: Chapter 22 of [1–3], and Section 19.3 of [4]. Somewhat older reviews are available in Mazumder [5] and Modest [6,7]. The purpose of this review article was to provide a more updated summary of the state-of-the-art and to do so in a manner wherein physical/mathematical models for the treatment of nongray radiation in combustion environments and methods for the subsequent solution of the ensuing governing equations are discussed in tandem.

Coupling radiation with other modes of heat transfer poses a challenge since radiative heat fluxes scale with the fourth power of temperature, while conductive and convective

Energies **2023**, 16, 4250 2 of 40

fluxes scale linearly with temperature. This makes the overall energy conservation equation strongly nonlinear whenever heat transfer by all modes is considered. Combustion systems pose additional challenges: the fuel and combustion products are generally strongly radiatively participating and significantly alter the radiation field. On the other hand, radiation alters the temperature field, and consequently, chemical reaction rates. Hence, an additional coupling with chemical kinetics (which is also strongly nonlinear) is manifested in such systems. Furthermore, the temperature and species concentration fields are rarely spatially or temporally uniform. Chemical species are created and locally destroyed by reactions, a process which is accompanied by the local creation or destruction of heat due to the reactions being exothermic or endothermic. Thus, to couple radiation with the other modes of heat transfer in combustion systems, one must account for the spatio-temporal variations in (1) species concentrations and their effects on local instantaneous radiative properties; and (2) the temperature field and its effect on both direct radiation emission and radiative properties.

Most practical combustion applications involve turbulent flow fields, wherein the aforementioned spatio-temporal variations in species concentrations and temperature occur at length and time scales that may span several orders of magnitude and are generally referred to as turbulent fluctuations. Fluctuations in temperature result in fluctuating radiative properties, which in turn, result in fluctuating radiative fluxes (or intensities). To capture the interactions between the fluctuating radiative properties and the radiation intensity—referred to as *turbulence-radiation interactions* (TRIs) [1,8,9]—special models are necessary. The potential interactions between various physical phenomena in a typical combustion environment are schematically depicted in Figure 1.

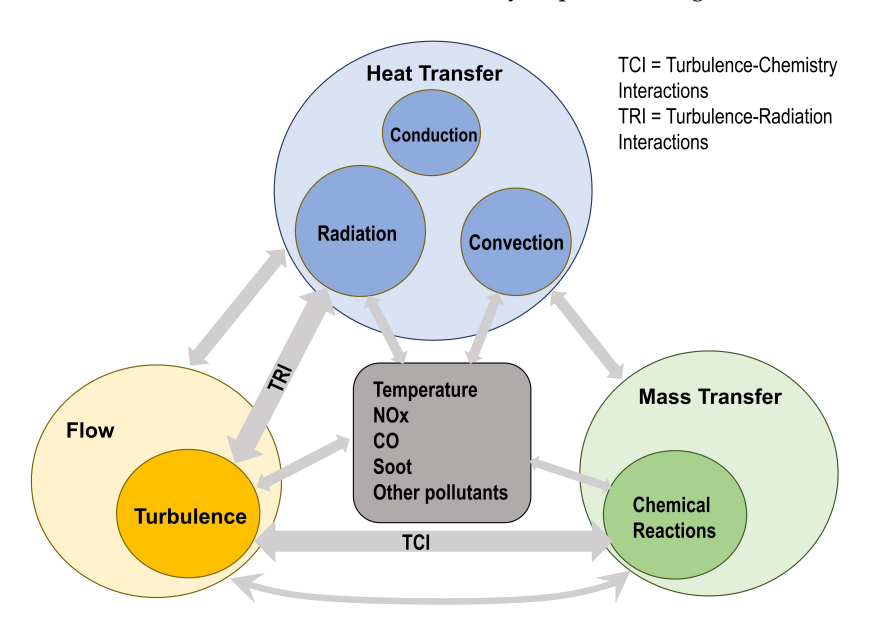


**Figure 1.** Interactions between various physical phenomena in a combustion environment. Double-ended arrows denote two-way coupling.

While accurately predicting temperature within a few tens of degrees has traditionally been deemed the metric for successful radiation or combustion computation, with growing emphasis on the reduction in pollutants in various engineering applications (internal combustion engines, gas turbine combustors, boilers, cement and steel production, among others), old criteria for judging the accuracy of such models need to be revisited. Since reaction rates are often related to temperature in a nonlinear manner, discrepancy in temperature predictions by a few percent can often lead to discrepancy in the prediction of pollutants, such as nitric oxide, by more than several tens of a percent, as shown later in Section 4.5. Such stringent requirements in accuracy warrant the development and use of sophisticated models for the treatment of radiation in combustion environments.

Energies **2023**, 16, 4250 3 of 40

The remainder of this article is organized as follows: in Section 2, the mathematical model (governing equations) pertinent to the treatment of radiation in combustion environments are presented. This is followed in Section 3 by a critical review of the radiative properties of molecular gases, particulates such as soot, and fuel droplets—sources for such data and how the extreme oscillatory behavior of these properties are treated in a modeling framework, i.e., nongray models. Section 4 reviews the state-of-the-art numerical methods and algorithms used to solve the nongray RTE and couple it to other physical phenomena, such as other modes of heat and mass transfer. The discussions of various combustion applications and the treatment of radiation in such contexts are split between Sections 3 and 4. The final section of the article—Section 5—delineates some of the current research challenges associated with modeling thermal radiation in combustion environments and perspectives for the future.

#### 2. Mathematical Model

In this section, the governing equations that need to be solved to model a combustion process are first presented. The radiative transfer equation (RTE) is covered in a separate subsection. The final subsection is dedicated to the treatment of turbulence in such systems.

## 2.1. Governing Equations

The governing equations are the equations of conservation of mass (both overall and individual species), momentum and energy. Although the scope of this review includes radiation in multiphase combustion systems, the equations presented here are for a single phase. The sole purpose of presenting these equations here is to elucidate the various couplings illustrated in Figure 1 in a mathematical sense. In a vectorial conservative form, the conservation equations for a single-phase gaseous system are written as [10–12]:

Overall mass: 
$$\frac{\partial}{\partial t}(\rho) + \nabla \cdot (\rho \mathbf{U}) = 0, \quad \ (1)$$

Momentum: 
$$\frac{\partial}{\partial t}(\rho \mathbf{U}) + \nabla \cdot (\rho \mathbf{U} \mathbf{U}) = -\nabla p + \nabla \cdot \boldsymbol{\tau} + \rho \mathbf{B}, \quad (2)$$

Energy (enthalpy): 
$$\frac{\partial}{\partial t}(\rho h) + \nabla \cdot (\rho \mathbf{U} h) = -\nabla \cdot \mathbf{q} + \dot{S}_h, \quad (3)$$

Species mass: 
$$\frac{\partial}{\partial t}(\rho Y_k) + \nabla \cdot (\rho \mathbf{U} Y_k) = -\nabla \cdot \mathbf{J}_k + \dot{S}_k, \quad \forall k = 1, 2, \dots, N,$$
 (4)

where p is the pressure,  $\rho$  is the mixture density,  $\tau$  is the shear stress tensor, and  $\mathbf{B}$  is the body force vector. Equations (1) and (2) are the so-called Navier–Stokes equations [10,11] and govern fluid flow. In Equation (4),  $Y_k$  is the mass fraction of the k-th species, and  $\mathbf{J}_k$  is the mass diffusion flux of the k-th species. The production rate of the k-th species due to homogeneous chemical reactions is denoted by  $\dot{S}_k$ . The total number of species in the system is denoted by N. In Equation (3),  $\dot{S}_h$  represents the net source due to viscous dissipation and other work and heat interactions, while h denotes the mixture enthalpy. It is related to the enthalpy of the individual species,  $h_k$ , through the relationship

$$h = \sum_{k=1}^{N} h_k Y_k. \tag{5}$$

In reacting systems, it is conventional [12] to include the thermochemical energy as part of the enthalpy of individual species (in addition to the sensible enthalpy), such that

$$h_k = h_{f,k}^0 + \int_{T_0}^T c_{p,k}(T')dT', \tag{6}$$

where  $h_{f,k}^0$  and  $c_{p,k}$  are the enthalpy of formation at the standard state and the specific heat capacity at a constant pressure of species k, respectively, and  $T_0$  is the standard-state

Energies 2023, 16, 4250 4 of 40

temperature. The enthalpy of individual species is generally available from standard thermodynamic databases, such as the NIST webbook or the JANNAF database. In Equation (3),  $\bf{q}$  denotes the net heat flux due to molecular diffusion (conduction), radiation, and interspecies diffusion, and is written as [10,11]

$$\mathbf{q} = \mathbf{q}_C + \mathbf{q}_R + \mathbf{q}_D = -k_C \nabla T + \mathbf{q}_R + \sum_{k=1}^N \mathbf{J}_k h_k, \tag{7}$$

where T denotes temperature and  $k_C$  is the thermal conductivity of the mixture. The species diffusion flux,  $J_k$ , is related to the species mass fraction,  $Y_k$ , through a phenomenological law. For binary systems or dilute systems, the Fick's law [10],  $J_k = -\rho D_k \nabla Y_k$ , may be used. For concentrated mixtures, Fick's law violates mass conservation, and it is more appropriate to use the Stefan–Maxwell equations [10]. A detailed discussion of these issues is beyond the scope of this article and may be found elsewhere [10,13,14]. In combustion modeling, Fick's law is traditionally used because most combustion applications (with the exception of oxy-fuel combustion) use air as the oxidizer, wherein nitrogen fractions are large enough for the mixture to be considered dilute. If the Fick's law is used, then Equation (7), when substituted into Equation (3), yields

$$\frac{\partial}{\partial t}(\rho h) + \nabla \cdot (\rho \mathbf{U} h) = \nabla (k_C \nabla T) - \nabla \cdot \mathbf{q}_R + \nabla \cdot \left[ \sum_{k=1}^N (\rho D_k \nabla Y_k) h_k \right] + \dot{S}_h. \tag{8}$$

Since the mixture enthalpy, h, is a function of the species enthalpy,  $h_k$ , through Equation (5), and the species enthalpy is, in turn, related to temperature through Equation (6), the left hand side of Equation (8) is clearly a function of T, albeit in a nonlinear way if the specific heat capacity is also considered a function of T. The examination of the right-hand side of Equation (8) reveals that all terms, except the radiation term,  $\nabla \cdot \mathbf{q}_R$ , are also functions of either T or one of the other unknowns in the system, namely  $\mathbf{U}$  (such as, viscous dissipation source) or  $Y_k$ . If radiation is disregarded, the system of equations given by Equations (1) through (8) are closed with 6+N unknowns (p,  $\rho$ ,  $\mathbf{U}(3)$ , T, and  $Y_k \forall k=1,2,\ldots,N$ ) and an equal number of equations, namely mass, with three momentum equations, an equation of state, energy (enthalpy), and N species conservation equations. If radiation is included, then the so-called radiation source,  $\nabla \cdot \mathbf{q}_R$ , must be somehow determined prior to the solution of Equation (8).

While it is known from thermodynamic principles (i.e., heat transfer, by definition, requires a temperature difference) that the radiative heat flux,  $\mathbf{q}_R$ , is a function of temperature, since radiation is a long-range or nonlocal phenomenon, unlike the conductive flux which is conveniently expressed by the Fourier law of heat conduction, it cannot be explicitly expressed in terms of temperature. In order to capture nonlocal phenomena (often referred to in the physics literature as *ballistic* effects), it is necessary to solve the so-called radiative transfer equation (RTE) [1], which is essentially the Boltzmann transport equation for photons.

## 2.2. The Radiative Transfer Equation (RTE)

The RTE describes the rate of change of radiation intensity with both time and space as caused by emission, absorption, and scattering. For terrestrial combustion applications, the length scales involved are small enough so that radiation transport, which occurs at the speed of light, may be considered instantaneous. As such, the radiation field reaches the steady state almost instantaneously and it is appropriate to just solve the steady-state form of the RTE, written as [1]

$$\frac{dI_{\eta}}{ds} = \hat{\mathbf{s}} \cdot \nabla I_{\eta} = \kappa_{\eta} I_{b\eta} - \kappa_{\eta} I_{\eta} - \sigma_{s\eta} I_{\eta} + \frac{\sigma_{s\eta}}{4\pi} \int_{4\pi} I_{\eta}(\hat{\mathbf{s}}_{i}) \Phi_{\eta}(\hat{\mathbf{s}}_{i}, \hat{\mathbf{s}}) d\Omega_{i}, \tag{9}$$

Energies **2023**, 16, 4250 5 of 40

where  $\hat{\mathbf{s}}$  is the unit direction vector along which the radiation intensity,  $I_{\eta}$ , propagates, and  $I_{b\eta}$  is the Planck function. The absorption and scattering coefficients of the media are denoted by  $\kappa_{\eta}$  and  $\sigma_{s\eta}$ , respectively, while  $\Phi_{\eta}$  denotes the scattering phase function.  $\Omega$  denotes the solid angle. The subscript  $\eta$  denotes the wavenumber, which is conventionally used in the gas radiation literature (as opposed to the wavelength) to denote spectral dependence. If the spectral absorption coefficient,  $\kappa_{\eta}$ , the spectral scattering coefficient,  $\sigma_{s\eta}$ , and the scattering phase function,  $\Phi_{\eta}$ , are known (these properties are discussed in detail in Section 3), then Equation (9) can be solved to obtain the spectral intensity  $I_{\eta}$ . Once the spectral intensity has been determined, the radiative heat flux and its divergence (radiation source) can be obtained using the following relationships [1]:

Radiative heat flux: 
$$\mathbf{q}_{R} = \int_{0}^{\infty} \int_{4\pi} I_{\eta} \hat{\mathbf{s}} \, d\Omega \, d\eta, \quad (10)$$
Radiation source: 
$$\nabla \cdot \mathbf{q}_{R} = \int_{0}^{\infty} \kappa_{\eta} \left( 4\pi I_{b\eta} - G_{\eta} \right) d\eta, = \kappa_{P} E_{b} - \int_{0}^{\infty} \kappa_{\eta} G_{\eta} \, d\eta, \quad (11)$$

where  $\kappa_P$  is the Planck-mean absorption coefficient, and  $E_b$  (=  $\sigma T^4$ ) is the blackbody emissive power. The so-called incident radiation is defined as [1]

$$G_{\eta} = \int_{4\pi} I_{\eta} \, d\Omega. \tag{12}$$

Whether radiation will be important in a combustion calculation largely depends on the optical thickness of the medium, which may be roughly estimated as  $\kappa_P L$ , where L is a characteristic length scale. Most laboratory-scale flames, for example, are too small for radiation to play a significant role in the accurate prediction of the temperature of the flame. For example, Figure 2 shows the predicted centerline temperature of the well-known Sandia Flame D with and without the inclusion of radiation in the model. For the original flame, the predictions with and without radiation differ only very slightly—the prediction including radiation agreeing better with experimental results. It is only when the flame size is scaled by a factor of 3 (Sandia D  $\times$  3) that significant differences in temperature are observed with and without radiation.

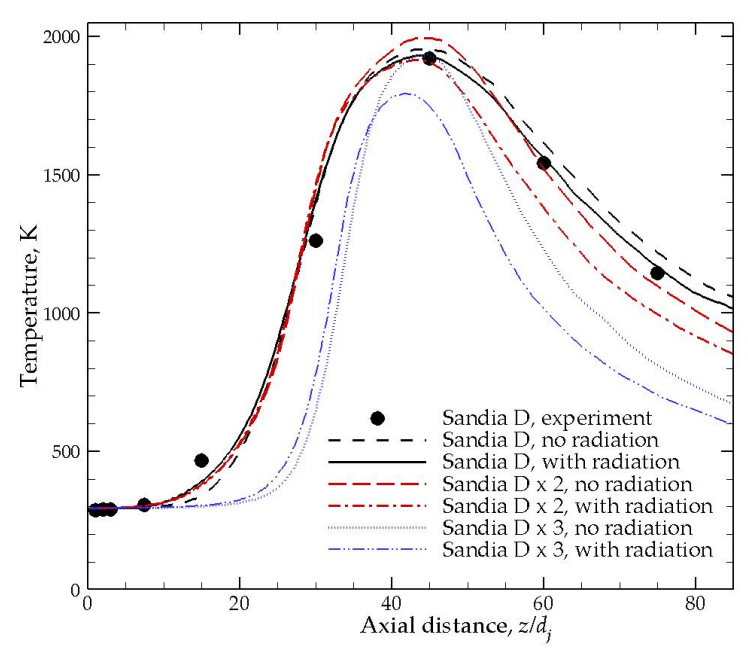


**Figure 2.** Effect of the inclusion of gas radiation in a methane-air jet diffusion flame on the centerline temperature of the flame; adopted from [15].

Energies 2023, 16, 4250 6 of 40

To summarize, the conservation equations of mass, momentum, energy, and species mass must be solved in conjunction with the RTE to model radiation in combustion systems. These equations are strongly coupled through multiple dependencies and some of them are nonlinear. Hence, a self-consistent iterative procedure is needed to solve them. Prior to the solution of the RTE in a combustion environment, it is necessary to obtain the radiative properties of the mixture that serve as inputs to the RTE. Furthermore, depending on how these properties vary across the spectrum, special models may be necessary to address the variations. This is the topic of discussion in the section to follow.

Most practical combustion applications involve turbulent flow. Although the governing equations presented in the two preceding sections are also valid in a turbulent flow field as well, the treatment of turbulence requires special consideration. In a turbulent flow field, the length and time scales span several orders of magnitude. For example, the smallest length scale—the so-called *Kolmogorov scale*—is approximately  $3 \times 10^{-7}$  m for a turbulent jet with a diameter of 1 cm (0.01 m) and a Reynolds number (based on the diameter) of one million. This implies that the resolution of all length scales in this particular situation would require  $0.01/3 \times 10^{-7} = 33,000$  grid points in the radial direction alone. Since turbulence is, by definition, three-dimensional (3D), the number of mesh points could potentially exceed  $33,000^3 \approx 3.6 \times 10^{13}$ . Such computations are referred to as direct numerical simulation (DNS), and are prohibitive for practical applications. Over the past half-century or so, a number of turbulence models have been developed to bypass the difficulties associated with DNS. These models treat the turbulent flow field in an approximate manner. Deterministic models for turbulence may be classified into two major categories: so-called Reynolds average Navier-Stokes (RANS) models and large eddy simulation (LES). In RANS, each independent variable is first split into a mean and a fluctuating part. These are then substituted into the governing equations and the resulting equations are then time-averaged. Unknown correlations between fluctuating quantities are then modeled to attain closure. In LES, the governing equations are solved on a grid that is somewhat larger than the Kolmogorov length scale so that the number of grid points are still tractable for practical computations. The physics at the scales below the grid scale (and larger than the Kolmogorov scale) is modeled using so-called subgrid-scale models. A detailed discussion of these approaches is well beyond the scope of this review article and the reader is referred to texts on turbulence [16,17]. Although LES has become increasingly tractable and grown in popularity over the past two decades, for combustion applications, wherein other complexities such as heat and mass transfer, and chemical reactions have to be modeled as well, the RANS approach, arguably, is more widely used. Stochastic approaches are also used to model turbulence. In such approaches, probability density functions (PDFs) that statistically characterize the turbulent field are employed—they are either assumed to be of some form or are substituted to the governing equations to develop new transport equations for the PDF, which are then solved using the Monte Carlo method. The approach—the so-called *transported PDF approach*—has been primarily brought to the limelight by Pope [18,19] for turbulent reacting flows.

## 2.3. Turbulence-Radiation Interactions (TRIs)

## 2.3.1. Types of TRI

The inclusion of radiation in turbulent combustion environments further complicates matters. The radiative properties of gases, particulates such as soot, and fuel droplets, namely the spectral absorption coefficient,  $\kappa_{\eta}$ , and spectral scattering coefficient,  $\sigma_{s\eta}$ , are generally strong functions of temperature [1]. The Planck function,  $I_{b\eta}$ , is also a strong function of temperature [1]. In a turbulent flow field, since the temperature fluctuates, it follows that all three of these quantities fluctuate. Since the spectral intensity,  $I_{\eta}$ , is related to these quantities through the RTE (Equation (9)), it also fluctuates due to turbulence. Fluctuations in the four aforementioned quantities due to turbulence couple in complex

Energies 2023, 16, 4250 7 of 40

ways that may be better understood by decomposing each of them into mean (average) and fluctuating parts following the RANS procedure:

$$I_{\eta} = \overline{I_{\eta}} + I'_{\eta}; \quad I_{b\eta} = \overline{I_{b\eta}} + I'_{b\eta}; \quad \kappa_{\eta} = \overline{\kappa_{\eta}} + \kappa'_{\eta}; \quad \sigma_{s\eta} = \overline{\sigma_{s\eta}} + \sigma'_{s\eta}.$$
 (13)

Most molecular gases are weak scatterers [1]. Hence, for the purposes of the present discussion on TRIs, we will assume that either scattering is negligible or that turbulence does not affect scattering. The substitution of Equation (13) into Equation (9) for a nonscattering medium, followed by time-averaging, yields

$$\frac{d\overline{I_{\eta}}}{ds} = \hat{\mathbf{s}} \cdot \nabla \overline{I_{\eta}} = \overline{\kappa_{\eta} I_{b\eta}} - \overline{\kappa_{\eta} I_{\eta}} = \overline{\kappa_{\eta} \overline{I_{b\eta}}} + \overline{\kappa_{\eta} I'_{b\eta}} + \overline{\kappa'_{\eta} I'_{b\eta}} + \overline{\kappa'_{\eta} I'_{b\eta}} - \overline{\kappa'_{\eta} I'_{\eta}} - \overline{\kappa'_{\eta} I'_{\eta}} - \overline{\kappa'_{\eta} I'_{\eta}} - \overline{\kappa'_{\eta} I'_{\eta}}.$$
(14)

Noting that the average of an average quantity results in the same quantity, the average of a fluctuating quantity is zero, and the average of the product of an average and fluctuating quantity is also zero; thus, Equation (14) reduces to

$$\frac{d\overline{I_{\eta}}}{ds} = \hat{\mathbf{s}} \cdot \nabla \overline{I_{\eta}} = \overline{\kappa_{\eta}} \overline{I_{b\eta}} + \overline{\kappa'_{\eta} I'_{b\eta}} - \overline{\kappa_{\eta}} \overline{I_{\eta}} - \overline{\kappa'_{\eta} I'_{\eta}}.$$
(15)

The comparison of Equation (15) with Equation (9) for just the emission terms divulges two important differences: (1) instantaneous quantities, such as  $\kappa_{\eta}$ , in Equation (9) got replaced by average of the same quantity in the corresponding terms in Equation (15), and (2) two extra terms, namely  $\overline{\kappa'_{\eta}I'_{b\eta}}$  and  $\overline{\kappa'_{\eta}I'_{\eta}}$ , appear in Equation (15). At this stage, these extra terms may be named as follows:

Emission TRI: 
$$TRI_e = \overline{\kappa_{\eta} I_{b\eta}} = \overline{\kappa_{\eta}} \overline{I_{b\eta}} + \overline{\kappa'_{\eta} I'_{b\eta}}$$
 (16)

**Absorption TRI**: 
$$TRI_a = \overline{\kappa_{\eta}} \overline{I_{\eta}} = \overline{\kappa_{\eta}} \overline{I_{\eta}} + \overline{\kappa'_{\eta}} I'_{\eta}$$
 (17)

Depending on the approach used to model the TRI terms, it may be convenient to either consider the first or the second expressions in the above two equations to account for the TRI in the RTE. The same two TRI terms also appear in the radiative source term for the overall energy equation. This is easily seen by time-averaging Equation (11), followed by the use of Equation (12), to obtain

$$\overline{\nabla \cdot \mathbf{q}_R} = 4\pi \int_0^\infty \overline{\kappa_\eta I_{b\eta}} \, d\eta - \int_0^\infty \overline{\kappa_\eta G_\eta} \, d\eta = 4\pi \int_0^\infty \overline{\kappa_\eta I_{b\eta}} \, d\eta - \int_0^\infty \int_{4\pi} \overline{\kappa_\eta I_\eta} \, d\Omega \, d\eta. \quad (18)$$

**Emission TRI.** As suggested by the name, the term emission TRIs was borne out of the emission term of the RTE, namely  $\kappa_{\eta}I_{b\eta}$ . The term emission TRI in Equation (18) may be alternatively written using the Planck-mean absorption coefficient [1] as

$$4\pi \int_0^\infty \overline{\kappa_\eta I_{b\eta}} \, d\eta = \overline{\kappa_P E_b},\tag{19}$$

To understand whether the emission TRI term augments or attenuates the radiation intensity, following the early work of Cox [20] and more recent work of Coelho [9], it is instructive to expand  $E_b$  using a Taylor series, such that

$$E_b(T) = E_b(\overline{T}) + T' \left[ \frac{dE_b}{dT} \right]_{T=\overline{T}} + \frac{1}{2} (T')^2 \left[ \frac{d^2 E_b}{dT^2} \right]_{T=\overline{T}} + \dots$$

$$= \sigma \overline{T}^4 + 4\sigma \overline{T}^3 T' + 6\sigma \overline{T}^2 (T')^2 + \dots$$
(20)

Energies 2023, 16, 4250 8 of 40

Then, multiplying Equation (20) by  $\kappa_P = \overline{\kappa_P} + \kappa_P'$ , and applying the rules of averaging, we obtain

$$\overline{\kappa_P E_b} \simeq \overline{\kappa_P} \sigma \overline{T}^4 \left[ 1 + 6 \frac{\overline{(T')^2}}{\overline{T}^2} + 4 \frac{\overline{\kappa_P' T'}}{\overline{\kappa_P} \overline{T}} \right],$$
(21)

wherein only up to second-order terms have been retained. The second and third terms within square brackets in Equation (21) represent contributions due to emission TRIs. Specifically, the second term, often referred to as the temperature self-correlation term, is a manifestation of the nonlinearity of the emissive power (or Planck function), i.e., the fact that  $\overline{\sigma T^4} \neq \sigma \overline{T}^4$ . Being proportional to the square of temperature fluctuations, this term is always positive and augments the radiation intensity. In a hypothetical scenario where the Planck-mean absorption coefficient is independent of temperature, pressure, and species concentrations, and does not fluctuate due to fluctuations in these quantities, the third term in Equation (21) would be absent. In such a case, the only possible effect of TRIs would be to augment the radiation intensity. In a real gas mixture, however, the absorption coefficient would fluctuate since it quite strongly depends on all three of the aforementioned quantities (see Section 3). In that case, in what way TRIs affect the radiation intensity would depend on how strongly  $\kappa'_p$  correlates with T' and whether the correlation is positive or negative. Previous studies [21,22] have indicated that emission TRIs are negligible in nonreacting flows, which suggests that the third term is negative and as strong as the temperature self-correlation term, although it is conceivable that both the second and third terms are weak in a nonreacting flow to begin with. In a relatively recent study of turbulent methane-air diffusion flames [23], it was shown that neglecting the third term overestimates the emission by the flame and takes it into account the decreased augmentation in intensity (and heat flux) by emission TRIs, suggesting that the correlation is negative in combustion scenarios. In another recent study, wherein these correlations have been assessed using transient data generated from the LES of pool fires [24], similar conclusions were reached.

In Equation (21), only terms up to the second order were retained. If the turbulent fluctuations are large, as is often the case in reacting flows, the neglected higher-order terms may be significant. In an effort to include the effect of higher-order terms, Snegirev [25] proposed the following model for emission TRIs:

$$\overline{\kappa_P E_b} \simeq \overline{\kappa_P} \sigma \overline{T}^4 \left[ 1 + 6C_{\text{TRI},1} \frac{\overline{(T')^2}}{\overline{T}^2} + 4C_{\text{TRI},2} \frac{\overline{\kappa_P' T'}}{\overline{\kappa_P} \overline{T}} \right], \tag{22}$$

Equation (22) differs from Equation (21) in that two new adjustable constants,  $C_{\text{TRI},1}$  and  $C_{\text{TRI},2}$ , which are to be determined by fitting the model predictions to experimental data, have been introduced. A value of  $C_{\text{TRI},1} = 2.5$  has been proposed [25], while the value of  $C_{\text{TRI},2}$  appears to be strongly problem-dependent and remains an open matter.

**Absorption TRI.** The term absorption TRI was borne out of the absorption term of the RTE, namely  $\kappa_{\eta} I_{\eta}$ . Absorption TRIs are difficult to model. Since radiation is a nonlocal phenomenon, the local intensity may be potentially influenced by the radiative property fluctuations from elsewhere in the medium. If the mean free path of the traveling photons are large compared to the size of the largest turbulent eddy, l, then local fluctuations in the radiative property only mildly affect the local intensity [26,27]. In such a scenario,  $\overline{\kappa_{\eta} I_{\eta}} \simeq \overline{\kappa_{\eta} I_{\eta}}$ . This expression is valid if only  $\kappa_{\eta} l \ll 1$  for all wavenumbers. It is commonly referred to as the *optically thin fluctuation approximation* (OTFA). The OTFA may be violated in combustion environments for very small parts of the spectrum where the absorption coefficient is unusually large and/or for extremely sooty flames. Studies show that it is justifiable in the vast majority of applications [8,28–33]. Most predictions of TRIs, to date, have employed the OTFA. Modest and coworkers [15,34–36] systematically investigated absorption TRIs in a number of nonluminous (nonsooting) and strongly sooting flames.

Energies 2023, 16, 4250 9 of 40

They found that, for nonsooting flames, absorption TRIs are almost always negligible. Even for laboratory-scale sooting flames, absorption TRIs were found to be unimportant; it became important (6% of emission TRI contributions) only when the flames were scaled artificially by a factor of 32 to increase their optical thickness. Recent studies in a sooty ethylene–air jet diffusion flame by Consalvi and coworkers [37] concluded that absorption TRIs are dominated by soot, but even in extreme cases (artificially scaling the laboratory-scale flame by a factor of 50), its effect on the radiative source is no more than 10%. Figure 3 shows the average spectral intensity leaving the flame for all wavenumbers for the scaled sooty flame. It is clear that, even in this case, absorption TRI contributions are small across the entire spectrum, thereby validating the fundamental assumption of the OTFA—that  $\kappa_{\eta}l \ll 1$  for *all* wavenumbers. A recent study of absorption TRIs in pool fires by the same researchers [38], wherein the optical thicknesses are much larger than laboratory-scale flames, however, shows that neglecting absorption TRIs significantly overpredicts the radiation loss from the flame and the OTFA is invalid.

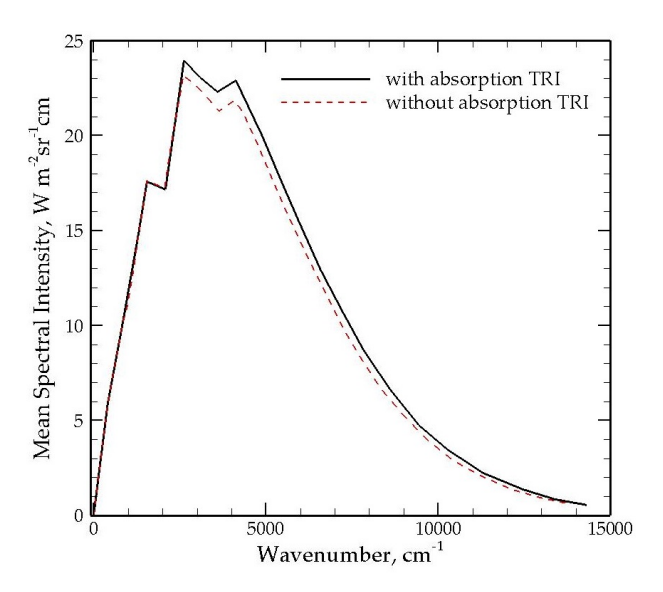


**Figure 3.** Effect of absorption TRI in a sooty ethylene-air jet diffusion flame artificially scaled up by a factor of 50; adopted from [37].

#### 2.3.2. Approaches to Modeling TRIs

RANS. Since emission TRIs are the dominant type of TRI in most combustion scenarios, significant research has been dedicated to modeling emission TRIs. One approach to do this is the RANS-based approach, wherein individual correlations arising out of averaging of the emission term, namely  $\kappa_P E_b$ , are modeled to various degrees of sophistication [23,31,32,39-45]. One approach to doing so is to assume PDFs that statistically describe the temperature and concentration fluctuations—an approach that has traditionally been used to address turbulence-chemistry interactions in flames [46,47]. The procedure for determining emission TRI correlations using assumed PDFs for temperature and concentration fluctuations is outlined in [9]. Clearly, the accuracy of such an approach is largely dependent on the PDF being assumed, and this issue has been investigated by Cumber and Onokpe [44]. In recent years, with LES becoming more viable, LES-generated data are being increasingly used to quantify emission TRI correlations. In a recent study, Fraga et al. [48] presented an improved emission TRI model wherein higher-order terms were retained but determined using LES-generated data for various diffusion flames. The higher-order correlations were related to the known or modeled lower-order correlations using curve-fits. This new model was found to outperform existing RANS-based emission TRI models, especially within the flame. The same researchers also used LES-generated data to better quantify emission TRIs for ethanol and methanol pool fires [24,49]. Their study concludes that, although temperature fluctuations are more important for the comEnergies 2023, 16, 4250 10 of 40

putation of the emission TRIs, fluctuations in the species' concentrations still need to be taken into account in order to obtain the accurate predictions of the mean radiative source. Absorption TRIs are difficult to model using the RANS approach because, unlike  $\overline{\kappa_P E_b}$ ,  $\overline{\kappa_\eta I_\eta}$  cannot be expressed in terms of other known two-point correlations and has, therefore, not been attempted.

**Transported PDF.** As mentioned earlier, in this approach, temperature and concentration fluctuations are described by PDFs, and transport equations for the PDFs are then developed and solved. This approach allows the direct determination of the TRI terms without having to decompose quantities of interest into mean and fluctuating components. The method has found extensive use in the treatment of turbulence–chemistry interactions in turbulent combustion computations [2,18,19]. In the realization of the fact that radiative property fluctuations are directly related to temperature and concentration fluctuations as much as in the case of reaction rate fluctuations, Mazumder and Modest [8,21] first proposed using this method to address TRIS. They considered TRIs in a methane-air diffusion flame as well as in a nonreacting combustion gas mixture. The so-called velocitycomposition joint PDF method [18] was used. A simple wide-band-based box model (see Section 3) was used to address the nongray nature of radiation. Absorption TRIs were neglected. The study of the nonreacting flow case [21] revealed that TRIs are negligible, which has also been confirmed by a recent DNS study [50] of a nonreacting water vapor jet. In contrast, in the methane-air bluff-body stabilized diffusion flame, the heat loss rate was found to increase by up to 75% [8] due to emission TRI effects. Since then, a large number of studies, primarily by Modest and coworkers [15,28,29,34-36], have investigated TRIs using this approach. These later studies used the composition PDF method, which combines a RANS solver for the flow field with a transported PDF approach for the scalar (temperature and concentration) field. A similar approach, commonly referred to as the Stochastic Eulerian Field approach [51], combines a RANS solver for the velocity field with steady flamelet models and a PDF for the mixture fraction and enthalpy. It has been extensively used by Consalvi and coworkers [32,33,37,51-53] for the study of TRIs in turbulent combustion environments.

LES and DNS. Over the past decade, LES has found increasing use in combustion applications. Its use for modeling TRIs is also becoming more routine. Chandy et al. [54] appear to have been the first to study TRIs using LES together with the so-called filtered density function (FDF) approach for modeling fluctuations at the subgrid scale. This preliminary study investigated an idealized luminous flame with a primitive soot model. It concluded that emission TRIs are always important at the subgrid scale. Absorption TRIs, on the other hand, can always be neglected at the subgrid scale. Roger et al. [55,56] conducted the DNS of stationary isotropic turbulence to arrive at the same conclusion. Gupta et al. [57,58] also used a combined LES-FDF approach but a much more sophisticated model based on the Monte Carlo method to address the strongly nongray nature of the radiating gases. Figure 4 shows instantaneous snapshots of a methane–air jet flame (Sandia Flame D scaled by a factor of 4) computed by Gupta [58]. Comparing Figure 4a,b, it is clear that the inclusion of radiation lowers the flame temperature by several hundred degrees. On the other hand, the comparison in Figure 4b,c shows that the flame in (c) is only slightly colder on an average, implying that a subgrid scale TRIs only has minor effect on the average temperature of the flame compared to grid-scale TRIs. More recent studies by Coelho [59] and by Consalvi et al. [60] also arrive at the same conclusion: subgrid-scale absorption TRIs is negligible, i.e., the OTFA can be reliably used at the subgrid-scale in LES computations. The extent to which emission TRIs are important at the subgrid scale remains debatable. Roger et al. [61] showed that if the filter scale, i.e., the length scale below which the turbulence is modeled, is approximately four times the typical grid size used in DNS calculations, then subgrid-scale emission TRIs are small (less than 5% of total emission). On the other hand, if the filter scale is 16 times the DNS grid size, then the subgrid-scale emission contribution can be as large as 35% of the total emission in some parts of the flame. However, the study also showed that this large fraction is in relatively colder parts of the

Energies **2023**, 16, 4250 11 of 40

flame where the emission is small to begin with. The exact same conclusion was reached in two recent studies [62,63]. It is for this reason that some LES computations [64] neglect the subgrid-scale TRIs in flame calculations altogether—both for emission and absorption. A recent investigation [38] of the same issue in pool fires, which have much larger optical thicknesses compared to laboratory-scale flames because of their size and the presence of appreciable amounts of soot, show that subgrid-scale emission TRIs can be quite important, while subgrid-scale absorption TRIs are still negligible.

A few DNS studies have also been conducted to study TRIs, despite being somewhat limited in scope. This is because, as previously discussed, TRIs become appreciable when the length scales (and optical thicknesses) are large, while the DNS of reacting flows with radiation can only be performed at relatively small (typically a few mm in size) computational domains due to the extreme computational cost. Nonetheless, an early study [65] performed DNS calculations for a statistically homogeneous mixing layer with the mixing of combustion gases. Recent studies include those by Kang [66], who simulated a premixed flame using DNS, but with a gray absorption coefficient; Rejeb and Echekki [67], who also assessed the TRIs in a gray medium similar to those in [66]; Armengol et al. [50], who conducted the DNS of a nonreacting water vapor jet, but with a detailed spectral Monte Carlo solver for radiation calculations; and Silvestri et al. [68], who also conducted DNS of a nonreacting flow in a channel with a detailed treatment of spectral radiation.

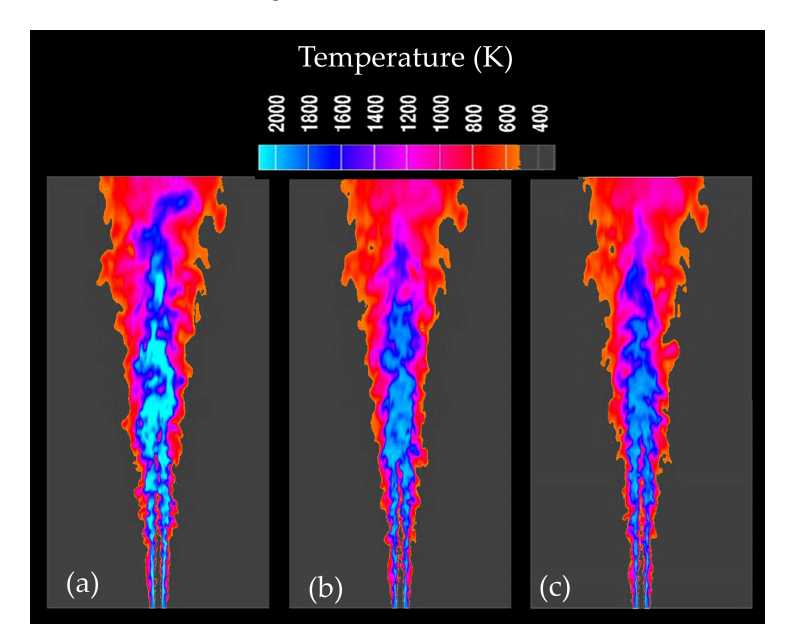


**Figure 4.** Results from LES-FDF computation of a methane–air jet flame: (a) without radiation, (b) with radiation and TRIs at the grid scale, (c) with radiation and TRIs at both grid and subgrid scales; adopted from [3,58].

## 2.4. Summary of Mathematical Model

To summarize, the governing equations that need to be solved to model a combustion process are presented in this section. First, the conservation equations of mass (both overall and individual species), momentum, and energy are presented. To address the radiation, the RTE must be solved, and this is presented next. The interaction between radiation and a turbulent flow field results in so-called TRIs. Various types of TRI were discussed and strategies to model them were presented.

#### 3. Spectral Radiative Properties

### 3.1. Gas Radiative Properties

Combustion environments are dominated by molecular gases that emit and absorb radiation in the visible and infrared parts of the spectrum. When a gas molecule is subjected to radiation (quantized as photons), it may either absorb the photons or scatter them.

Energies **2023**, 16, 4250 12 of 40

Absorption raises the energy level of the molecule. Since quantum mechanics postulates that energy levels are discrete or quantized, only photons with a certain energy or frequency (noting that the energy of a photon is given by  $E = h\nu$ , where h is the Planck constant and  $\nu$  is the frequency) can be absorbed. Likewise, only photons of certain frequencies can be emitted when transitions occur from higher to lower energy levels. Consequently, the absorption and emission spectra of most molecular gases exhibit a strong line structure. Depending on the exact structure of the molecule, these lines may form dense clusters, often referred to as bands. The detailed discussion of the absorption and emission spectra of molecular gases is beyond the scope of this article, and the reader is referred to texts [1,4] for such a discussion. For the purposes of this review, it is sufficient to state that, over the past five decades or so, the position (in the frequency or wavenumber space) and strength (line height and width) of these lines have been recorded using a combination of ab initio calculations and spectroscopic measurements and are now available in the form of wellknown databases. The most well known of these databases is the HITRAN database, which was originally developed to facilitate atmospheric radiation calculations, and is currently in its 2020 version [69]. In high-temperature combustion environments, new lines appear in the absorption/emission spectra as a result of transitions to and from higher energy levels. The HITEMP database, which is currently in its 2010 version [70], was developed to account for these new lines, and is routinely used for radiation calculations in high-temperature applications. Another popular database, dedicated to carbon dioxide and typically used for combustion applications, is the CDSD database [71,72], with the latest version being from 2011 [72].

The calculation of the spectral absorption coefficient from the line information contained in the aforementioned spectroscopic databases requires accounting for various line broadening mechanisms and partition functions, and is discussed in detail in Chapter 10 of [1]. Figure 5 shows the spectral absorption coefficient of pure carbon dioxide at two different temperatures and at 1 bar, computed using the HITEMP database for just ten wavenumbers. It is quite evident that even for the small wavenumber range of 10 cm<sup>-1</sup> shown in the figure, the absorption coefficient oscillates strongly, particularly at a high temperature. Since the determination of the net radiative heat flux and its divergence (radiation source) requires a spectral integration, as evident from Equations (10) and (11), it follows that the accurate determination of these quantities will require splitting the spectrum into extremely tiny wavenumber intervals within which the absorption coefficient may be assumed to be constant. For each tiny spectral interval, the RTE will have to be solved separately to obtain the spectral intensity and, subsequently, summed to obtain the net heat flux or radiation source. Such calculations are referred to as line-by-line (LBL) calculations. Depending on the temperature range and the gases involved, a spectral interval of 0.01–0.001 cm<sup>-1</sup> is required for accurate LBL calculations. Since radiative energy in typical combustion applications span several thousands of cm<sup>-1</sup>, it follows that LBL calculations in combustion environments will typically require the solution of the RTE for more than a million times. Hence, such calculations are not viable for practical problems and are generally conducted to generate benchmark results for the verification of approximate spectral (nongray) models in very simple configurations—typically, one-dimensional (1D) homogeneous gas layers. These benchmark results are scattered within individual publications. Recently, efforts have been made to disseminate such benchmark results separately for multidimensional enclosures [73] with a mixture of CO<sub>2</sub>, H<sub>2</sub>O, and N<sub>2</sub>. An adaptive LBL spectral integration scheme, which claims to reduce the computational time of LBL calculations by a factor of three to five while retaining LBL accuracy, was also recently proposed [74].

Energies **2023**, 16, 4250 13 of 40

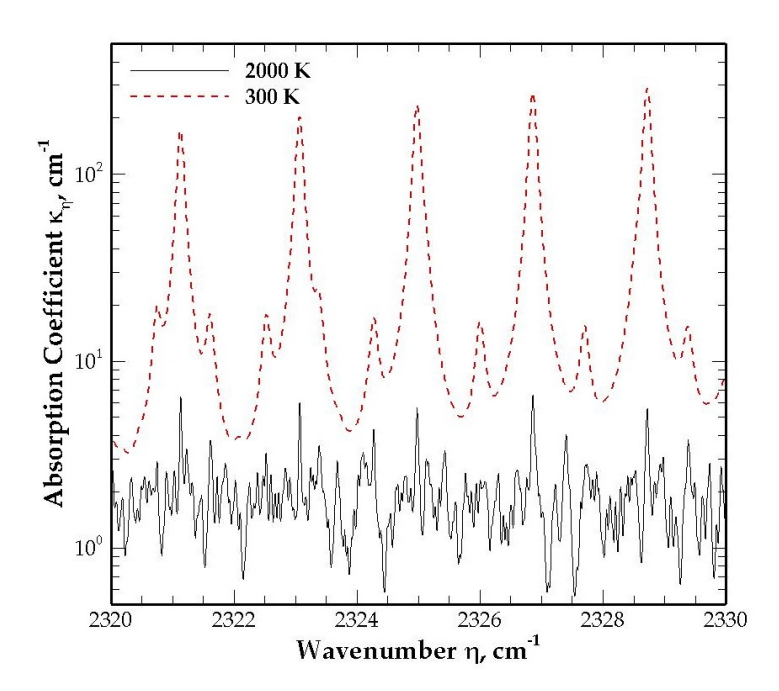


**Figure 5.** Spectral absorption coefficient of pure carbon dioxide at 1 bar and at two different temperatures computed using the HITEMP 2010 database.

#### 3.2. Radiative Properties of Soot

Unlike most combustion gases, particulates tend to introduce significant scattering effects in radiative transfer. The radiative properties of particles are characterized by the absorption and scattering cross-sections of the particles [1]. The absorption and scattering cross-sections are, in turn, calculated using an appropriate theory (such as Mie theory, Rayleigh theory, or Rayleigh–Debye–Gans theory) based on the optical properties of the particle material (indicated by its complex index of refraction, m = n - ik) and the morphology of the particle (indicated by size, shape, fractal nature, etc.) [75]. Of all the particulates relevant to radiation calculation in combustion systems, soot is arguably the most important one. The attempt to understand the radiative properties of soot is of interest to not only the combustion community but also to the atmospheric science community as soot is one of the major radiative forcing agents for the global climate. Soot particles are found in flames as aggregates of polydispersed primary particles. The size of the primary particles, as characterized by their mobility diameter, can vary from a few nanometers to upwards of 20 nm [76], whereas the mobility diameter of soot aggregates can be as large as a few hundreds of nanometers [77]. As primary particles age from nascent to mature soot, their absorption cross-section and emissivity increase and broaden to cover a wide spectrum [78–81]. In the atmospheric science community, mature soot is often referred to as black carbon owing to its strong absorbance [77,81]. The knowledge gap in our understanding of the properties and structures of soot particles—be it primary particles or aggregates—is still significant.

Since soot primary particles are usually small enough to fall under the scope of Rayleigh theory [1], the spectral absorption coefficient of soot primary particles can be calculated using an "absorption function" or "refractive index function" denoted as E(m) in Equation (23):

$$\kappa_{\lambda} = 6\pi \left( \frac{6nk}{(n^2 - k^2 + 2)^2 + 4n^2k^2} \right) \frac{f_v}{\lambda} = 6\pi E(m) \frac{f_v}{\lambda},$$
(23)

where  $f_v$  is the soot volume fraction. However, measurements indicate that the variation in the soot absorption coefficient does not vary with the inverse of the wavelength, as

Energies 2023, 16, 4250 14 of 40

suggested by Equation (23). To account for this, the soot absorption coefficient is often represented using two empirical constants: *C* and *a* are as shown in Equation (24):

$$\kappa_{\lambda} = \frac{Cf_{v}}{\lambda^{a}} \tag{24}$$

The constant a is referred to as a "dispersion exponent" or "Angström exponent." Starting from the 1960s and continuing until today [82–87], attempts have been made to determine these radiative and optical properties (i.e., dispersion exponent, m, E(m), etc.) of soot. For example, Figure 6 shows a comparison of the measured complex index of the refraction from three independent studies. Excellent reviews of radiative property data for soot are available in the literature [75,88].

Under the small particle limit of Rayleigh theory, the scattering by unaggregated soot particles can be neglected [1]. However, Rayleigh theory is not appropriate for large particles or soot aggregates. Recent studies have shown that a reasonable estimate of the absorption and scattering cross-section of soot aggregates can be obtained using tools such as generalized a multiparticle Mie solution, superposition T-matrix, Rayleigh–Debye–Gans theory, or the discrete dipole approximation [80,88,89]. However, most of these studies have been conducted with the development of accurate diagnostic techniques in mind and their use in combustion simulations remains very limited due to the limitations of state-of-the-art soot models in continuum-scale combustion simulations. Therefore, in this review, we will not focus on these developments on soot radiative and optical property estimation; instead, we point the interested reader to the excellent review conducted by Liu et al. [88].

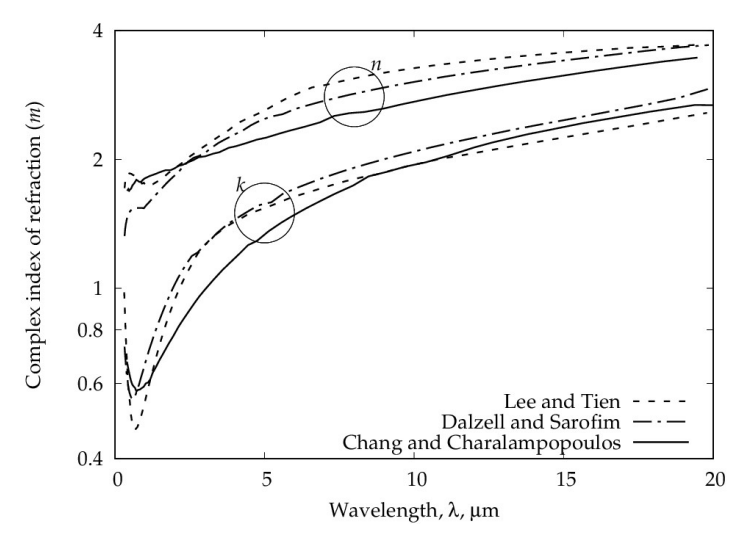


**Figure 6.** The measured complex index of refraction for soot from Lee and Tien [85], Dalzell and Sarofim [84], and Chang and Charalampopoulos [86]; adopted from [1].

## 3.3. Radiative Properties of Fuel Droplets

While particulates such as soot are almost always treated as an extension of the continuum-scale gas-phase flow, liquid droplets—as found in spray combustion—are often treated as a discrete phase in a gaseous carrier medium. This is due to the much larger size of the droplets (typically,  $\mu$ m-mm) than soot particles. This larger size makes the treatment of radiation in droplets considerably different than that of soot particles. At the same time, the spherical shape of droplets allows the direct application of Lorenz–Mie theory for droplet radiation if the complex index of refraction is known [1]. In this review, we only focus on the radiative properties of fuel droplets. There have also been some studies on the water droplets and their interaction with the combustion environments, primarily in the context of fire mitigation and safety (e.g., [90–95]), but those studies are beyond the scope of this review.

Energies 2023, 16, 4250 15 of 40

Many studies have been dedicated to the extraction of the complex index of refraction of liquid fuels of relevance. Many of these studies are focused on single-component fuels. For example, data are available from several researchers on the spectral variation of the complex index of refraction of iso-pentane [96], iso-octane [96], n-hexane [96], n-heptane [96–98], n-nonane [96], n-decane [96–99], n-hexene [96], o-xylene [96], and toluene [96], isopropanol [99], and n-butanol [99]. Although many of these components are the components of real fuels, the radiative properties of real fuels such as Diesel vary noticeably from these components. Dombrovsky and coworkers [100–102] have studied the spectral complex index of the refraction of different grades of Diesel and noted that the index of absorption varies more prominently than the index of refraction with the grade and condition of the fuel. Figure 7 shows the variation in n and k for n-heptane and a specific grade of Diesel fuel.

For large droplets, the size parameter (i.e., a ratio of its radius, a, and wavelength of radiation,  $\lambda$ , denoted by  $x=\frac{2\pi a}{\lambda}$ ) is often large enough that they fall under the regime of geometric optics [1]. Depending on the ratio of the droplet vs. size parameter, x, and the index of absorption, k, it can be treated as either semi-transparent ( $k \ll 1, x \gg 1$ ) or opaque ( $kx \gg 1$ ). While the application of Mie theory can provide an exact evaluation of a droplet vs. absorption and scattering efficiencies, the calculations can be very computationally tedious. To avoid this, Dombrovsky and coworkers [100,103] have also proposed an approximate scheme by curve-fitting the Mie solutions for droplets under a variety of configurations.

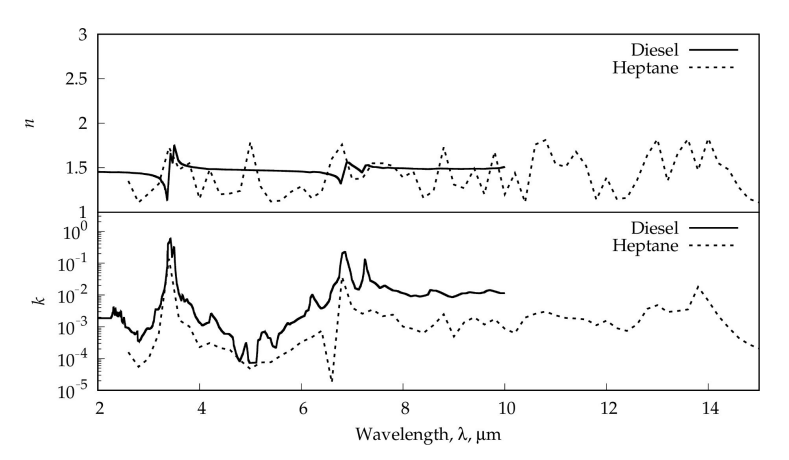


**Figure 7.** Measured complex index of refraction for n-heptane [98] and Diesel (unboiled) [100]; adopted from respective references.

#### 3.4. Spectral (Nongray) Models

As discussed in Section 3.1, deterministic LBL calculations are only feasible in extremely simple scenarios. For computations in practical combustion systems, models that address the extreme nongray nature of typical combustion gases and particulates are necessary. For over six decades, a number of models have been developed and used to treat nongray radiation in gases. A discussion of the mathematics, assumptions, and nuances underlying each model is well beyond the scope of this review, and is available in advanced texts on radiative heat transfer, such as Chapters 10 and 19 of [1] and Chapter 9 of [4]. Here, only a brief overview of the most popular methods is presented.

**Wide-band (WB) models.** As discussed earlier, depending on the exact structure of a molecule, the energy levels associated with the vibration and/or rotational transitions may be different and often grouped together closely, resulting in so-called vibration–rotation bands. These groupings may span several hundred cm<sup>-1</sup> in wavenumber space; hence, the name *Wide Band*. Wide-band models are one of the earliest to be developed. Their primary purpose is to accurately predict the net emission and absorption over an entire band, rather than at each wavenumber. This is useful since the calculation of the net radiative heat transfer rate or its divergence (radiation source) requires integration over

Energies 2023, 16, 4250 16 of 40

the spectrum anyway. Wide-band models make use of the fact that the Planck function change is marginal across a wide band. Two different variations of wide-band models have found widespread use: (1) the box model or step-wise gray model, and (2) the exponential wide-band model. In the box model [104], the band is approximated as a rectangular box with a width of  $\Delta \eta$  and a height of  $\overline{\kappa}$ , such that the product  $\overline{\kappa}\Delta \eta$  matches the so-called band intensity. The box width is generally selected and the band height is consequently determined. The selection of the box width is a topic of much debate and discussion and it is well known that its choice significantly affects the accuracy [1]. Nonetheless, this model is quite popular for engineering calculations, and continues to be used [5,8,21,105,106]—one notable advantage being that the  $\overline{\kappa}$  values for each band can be directly used within the general form of the RTE. Exponential wide-band models assume that the line strengths decrease exponentially from the band center. This assumption, coupled with the fact that the Planck function variation is benign over a wide-band, allows relatively straightforward integration to compute the so-called band absorbance. Detailed description on how to do this using parameters for various bands for various combustion gases (which are tabulated) is available in [1,107]. The exponential wide-band model does not provide the absorption coefficient of the gas or gas mixture in question. It can only be used in conjunction with the RTE if additional approximations are made to extract the absorption coefficient—one of the common ones being the box model approximation. In other words, the exponential model is first used to compute the band absorbance. This is then followed by use of the box model to compute  $\overline{\kappa}$ , which can then be directly used within the RTE. Additional approximations are needed to treat nonhomogeneous media, resulting in further loss of accuracy. These various assumptions and approximations can often lead to errors in radiation source or radiative heat flux predictions of more than 70% [1].

Narrow-band (NB) models. In narrow-band models, spectral integration is conducted over narrow bands, typically spanning a few tens of wavenumbers to compute the average emissivity or transmissivity of the band. As shown in Figure 5, even with such a small part of the spectrum, the absorption coefficient can oscillate wildly. Thus, a model is necessary to better describe the position and strength of the lines within the narrow band. Several models have been used for this purpose. These include the Elsasser model, the Goody model, or the Malkmus model. Another approach is to reorder the lines within the narrow band to construct so-called k-distributions, which allow accurate integration over the narrow band. These various models and how to calculate narrow-band transmissivities using these models are discussed in [1]. Databases that report narrow-band parameters and properties (emissivity and transmissivity) have been developed, the two most popular ones being RADCAL [108] and the more recent EM2C [109,110], which is constructed using LBL data and the Malkmus model. Much like wide-band models, narrow-band models do not directly provide the narrow-band absorption coefficient, unless approximations such as those in the aforementioned box model are made. Consequently, narrow-band models are not amenable to the general solution of the RTE. In a recent publication [111], a formulation that allows the accurate calculation of the narrow-band absorption coefficient from commonly stored (in databases) narrow-band parameters has been presented.

Weighted-sum-of-gray-gases (WSGG). In the WSGG model, it is hypothesized that the effect of a nongray gas can be accurately represented by the combined effect, i.e., the weighted sum of a set of gray gases. Each gray (fictitious) gas can be treated independently. Originally developed to calculate the total emissivity, the method was later generalized by Modest [112] to make it compatible with the general RTE. The fundamental challenge in the WSGG model lies in determining the weights and absorption coefficients of the various gray gases. With the advent of the spectroscopic databases mentioned in Section 3.1, significant research has gone into fine-tuning this model. These include a refinement of the gray-gas weights based on data in newer spectroscopic databases [113,114], the extension to a higher temperature and the pressure [115,116], extension to accommodate oxy-fuel combustion [117], and the extension to include soot [118–120]. It continues to have great popularity for combustion applications [121–124].

Energies **2023**, 16, 4250 17 of 40

Spectral-line-based weighted-sum-of-gray-gases (SLW). In the SLW model, pioneered by Denison and Webb [125], the entire absorption cross-section (absorption coefficient scaled by the inverse of the molar density) range is broken up into a set of gray gases (i.e., gases with constant absorption coefficients). These gray-gas absorption coefficients are determined by performing a logarithmic average of the adjacent so-called supplemental absorption cross-sections multiplied by the molar density. Using this model, the RTE essentially transforms to the same form as that in the WSGG model. The main difference is that, in the SLW model, the weights of the various gases are determined by taking the difference between the values of the absorption-line blackbody distribution function (ALBDF) at the adjacent supplemental absorption cross-sections. This makes the method essentially "exact," i.e., the LBL accuracy can be reproduced with a sufficient number of gray gases. The method underwent several improvements in its early stages: the extension to nonhomogenous media [126], new formulations for gas mixtures [127,128], and extension to soot [129]. Later versions introduced the so-called rank-correlated SLW [130]. The SLW method and its variants have found prolific use for the accurate computation of nongray radiation in combustion systems [131–134].

**Full-spectrum** *k***-distribution (FSK).** The concept of a *k*-distribution was first introduced for atmospheric radiation transport calculations [135]. Within a narrow-band, the absorption coefficient of molecular gases oscillate wildly, often hitting the same absorption coefficient value multiple times for different wavenumbers, as shown in Figure 5. This multiplicity behavior allows the reordering of the absorption coefficients in increasing or decreasing order to generate a smooth so-called k-distribution. The spectral integration of the product of the oscillating absorption coefficient and any other smooth quantity, as required for the computation of the radiative heat flux or radiation source (see Equations (10) and (11)), can then be transformed into an integration of the product of the smooth k-distribution and another smooth function. This allows the very efficient and accurate numerical integration with just a few quadrature points. This idea was further extended by Modest and Zhang [136] to the full spectrum, resulting in the so-called full-spectrum k-distribution (FSK) method. The method produces almost LBL accuracy with less than 10 quadrature points (number of times the RTE needs to be solved) for homogeneous media. For nonhomogeneous media, the accuracy depends on how well the k-distributions upon different conditions correlate. This has resulted in the so-called full-spectrum correlated k-distribution (FSCK) method. Over the past two decades, significant research has gone into extending the FSK method to nonhomogeneous media with and without soot, and liquid fuels [137–143], nongray walls [144,145], and k-distribution databases constructed from LBL and narrow-band data have been created and disseminated [146,147]. Today, in its third edition, the FSK model is one of the most accurate, efficient, and popular models for the computation of nongray radiation in combustion environments [148–150].

**Models for soot.** In combustion simulations, the most common approach almost always neglects scattering by soot particles, following the Rayleigh limit. It should be noted here that although Rayleigh theory is often invoked in modeling soot radiation, its applicability may not always be true, particularly in the limit of large primary particles. The absorption coefficient of soot particles is often calculated using Equation (23) with an appropriate value for m. While Equation (23) includes wavelength dependence via the factor  $1/\lambda$ , the nongray or spectral nature of soot comes via the spectral variation of its optical property (i.e., m). A popular option for the complex index of refraction of soot is to use a constant value for m making the treatment, in the strictest sense, gray. An excellent review of the different values of a complex index of refraction can be found in [75]. A common choice for the complex index of refraction for soot in combustion simulations is m = 1.57 - 0.6i, as proposed by Smyth and Shaddix [151].

Energies **2023**, 16, 4250 18 of 40

On the other hand, a correlation proposed by Charalampopoulos and Chang [86] remains a convenient and popular choice for the wavelength-dependent formulation of m, and is given by

$$n(\lambda) = 1.811 + 0.1263 \ln(\lambda) + 0.027 \ln^2(\lambda) + 0.0417 \ln^3(\lambda), \tag{25}$$

$$k(\lambda) = 0.5821 + 0.1213 \ln(\lambda) + 0.2309 \ln^2(\lambda) - 0.01 \ln^3(\lambda), \tag{26}$$

where the wavelength  $\lambda$  is measured in  $\mu m$ . The correlation, as shown in Equations (25) and (26), is valid in the range of 0.4–30  $\mu m$ .

Summary of spectral models. A review of the recent literature reveals that the FSK and SLW models are two of the most popular models for modeling nongray radiation in combustion environments [3,152]. In a recent article [149], it has been shown that the SLW and FSK models share many commonalities. Although these two models are frontrunners, the WSGG model continues to be quite popular with its many recent improvements and updates, especially for coal combustion and other applications involving soot and/or high pressure [116,118,119]. Another model that has found some use is the narrow-bandbased k-distribution model or NBCK [152–154]. NBCK is computationally far more (>20×) expensive than either FSK or SLW, but has the best accuracy among all methods. Consequently, in recent studies of actual flames and fires, for which LBL calculations are all but impossible, NBCK results were used as benchmark results for assessing other models when two-way coupling with radiation is included [152]. Figure 8 shows a comparison of the accuracy of the latest versions of the FSCK, the rank-correlated SLW, and the WSGG models for the computation of the radiation source in a turbulent diffusion flame at two different pressures [152]. The reference solution was computed using the NBCK model with 128 Gaussian quadrature points, and the errors are with respect to this reference solution. It is clear that the FSCK and SLW models have comparable accuracy, while the WSGG model is somewhat less accurate than these two frontrunners. A newly developed transmissivity-based spectral model—an ℓ-distribution model [155]—also showed a good level of accuracy in a recent study [156]. Although somewhat obsolete and not as accurate, step-wise gray (or box) models based on either narrow-band or wide-band data continue to be used [105] for modeling combustion in practical systems because of their ease of use and implementation—notably, most commercial CFD codes provide an in-built step-wise gray model framework.

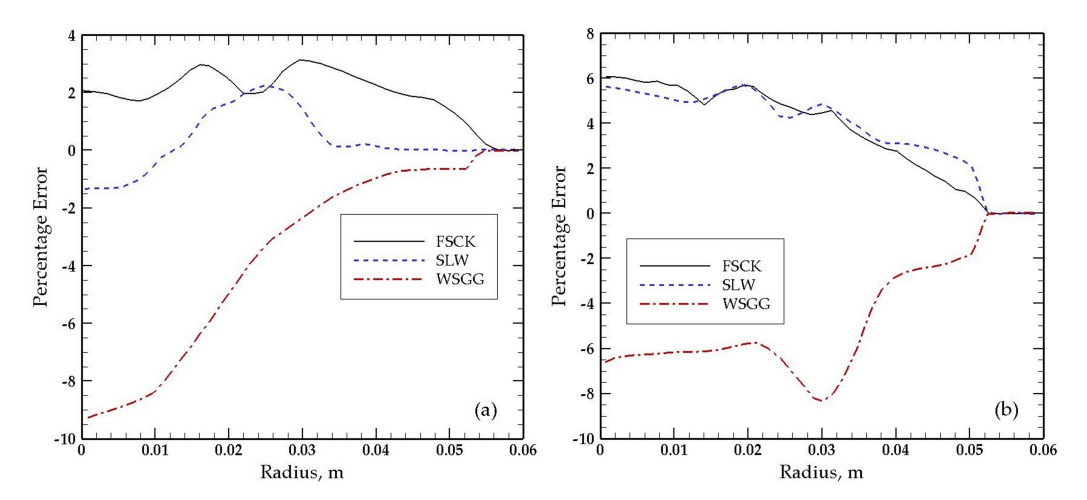


**Figure 8.** Comparison of the accuracy of three popular spectral models for the prediction of the radiation source in a methane-air turbulent jet diffusion flame at two different pressures: (a) 1 atm; and (b) 4 atm; adopted from [152].

Energies 2023, 16, 4250 19 of 40

#### 3.5. Summary of Spectral Radiative Properties

In this section, the spectral radiative properties pertinent to combustion environments were discussed: molecular gases, soot, and fuel droplets. Since the spectral radiative properties of most combustion gases oscillate wildly across the spectrum, so-called nongray models are necessary to address their impact on the radiation field. A brief overview of the various spectral (nongray) models used to date was presented along with a critical discussion of their pros and cons.

#### 4. Solution of the RTE

As mentioned earlier, the RTE is a five-dimensional integro-differential equation, with the wavenumber being an additional parameter, i.e., it has to be solved for multiple wavenumbers. As discussed in Section 3, in combustion environments, this is particularly challenging because of the extreme spectral variation of radiative properties, making it a top priority to find an efficient solution to the RTE. Both deterministic and stochastic (Monte Carlo) techniques have been developed for the solution of the RTE, and both are widely used. In the two following subsections, the two most popular deterministic methods for solving the RTE, namely the method of spherical Harmonics ( $P_N$  approximation) and the discrete ordinates method ( $S_N$  approximation) and its latest variants are presented. This is followed by an overview of the Monte Carlo (MC) method and latest developments of the MC method for the solution of the nongray RTE. Finally, a short subsection that discusses hybrid methods is included.

#### 4.1. $P_N$ Approximation

What makes the RTE so challenging to solve compared to the conservation equations of mass, momentum, and energy is its directional nature. In Cartesian coordinates, for example, the spectral radiation intensity in Equation (9) is a function of five independent variables:  $I_{\eta} = I_{\eta}(x,y,z,\theta,\psi)$ , where (x,y,z) are the three independent spatial coordinates, while  $(\theta,\psi)$  are the two independent angular coordinates. In the method of spherical harmonics ( $P_N$  approximation), a linear combination of spherical harmonic functions is used to analytically represent the angular variation of intensity. A detailed discussion of the general  $P_N$  formulation is well beyond the scope of this article and may be found elsewhere [1,157]. Here, only the lowest order, namely the  $P_1$  approximation, is discussed briefly, primarily because it has found prolific usage for the solution of the RTE in combustion applications. In the  $P_1$  approximation, the spectral intensity at any location,  $\mathbf{r} = \mathbf{r}(x,y,z)$ , and in any direction,  $\hat{\mathbf{s}} = \hat{\mathbf{s}}(\theta,\psi)$ , is written as a linear function of the direction vector  $\hat{\mathbf{s}}$ :

$$I_{\eta}(\mathbf{r},\hat{\mathbf{s}}) = J_{0,\eta}(\mathbf{r}) + [J_{1,\eta}(\mathbf{r})] \cdot \hat{\mathbf{s}}, \tag{27}$$

where  $J_{0,\eta}(\mathbf{r})$  is a space-dependent scalar coefficient, while  $\mathbf{J}_{1,\eta}(\mathbf{r})$  is a space-dependent vector coefficient. The substitution of Equation (27) into Equation (9) for a linearly anisotropically scattering medium, followed by extensive mathematical manipulation, yields [1]

$$\nabla \cdot \left[ \frac{1}{\beta_{\eta} - A_1 \sigma_{s\eta} / 3} \nabla G_{\eta} \right] - 3\kappa_{\eta} G_{\eta} = -12\pi \kappa_{\eta} I_{b\eta}, \tag{28}$$

where  $A_1$  is the coefficient in the scattering phase function for linear anisotropic scattering, and  $\beta_{\eta}$  (=  $\sigma_{s\eta} + \kappa_{\eta}$ ) is the extinction coefficient. Likewise, Equation (27) can be substituted into the boundary condition for the RTE, and following the so-called Marshak procedure [1], we obtain

$$-\frac{2-\epsilon_{w\eta}}{\epsilon_{w\eta}}\frac{2}{3\beta_{\eta}-A_{1}\sigma_{s\eta}}\hat{\mathbf{n}}_{w}\cdot\nabla G_{\eta}+G_{\eta}=4\pi I_{bw\eta},\tag{29}$$

where the extra subscript, w, denotes the quantities evaluated at the wall (or boundary), and  $\hat{\mathbf{n}}_w$  is the unit surface normal at the wall pointing from the wall to the medium next to

Energies 2023, 16, 4250 20 of 40

it. Equation (28) is a linear elliptic partial differential Equation (PDE) that can be readily solved, subject to the boundary condition given by Equation (29) using standard spatial discretization techniques such as the finite-difference, finite-volume, or finite-element methods. Most importantly, the directional dependence of the original RTE (Equation (9)) has now disappeared from Equation (28), making it straightforward to solve. One important point to note is that, if the medium is completely transparent, i.e.,  $\kappa_{\eta} = \sigma_{s\eta} = \beta_{\eta} = 0$ , then Equation (28) becomes singular, i.e., the  $P_1$  approximation cannot be used for the parts of the spectrum where the medium is transparent. Since the  $P_1$  approximation expresses the intensity as a linear function of direction, the method cannot accurately treat intensity fields that are strongly directional, such as in an optically thin medium bounded by a combination of walls of very different temperatures. Nonetheless, the simplicity of the  $P_1$  equation and its solution makes it one of the most attractive choices for solving the RTE.

In combustion applications, wherein emission by the reaction zone is often dominant, the P<sub>1</sub> approximation tends to produce reasonably accurate results. A large number of researchers have used and assessed the  $P_1$  and other higher-order  $P_N$  approximations for combustion applications [5,8,105,158-163]. In [5,8], the  $P_1$  approximation was used in conjunction with the step-wise gray model to treat radiation and TRIs in a bluff-body stabilized methane-air flame. In [158], Cai et al. studied laminar hydrogen-air diffusion flames. The RTE was solved using the P<sub>1</sub> approximation, and two higher-order versions of the so-called *simplified*  $P_N$  approximation, namely the  $SP_3$  and  $SP_5$  approximations. The FSCK model was used as the nongray model. Results show that the higher-order approximations, namely SP3 and SP5, did not offer any particular advantage in terms of accuracy over P<sub>1</sub>. The exception was when the pressure was raised to 30 bar, when SP<sub>5</sub> outperformed the other two solvers. The three solvers were found to be comparable in terms of computational cost. Garten et al. [159] performed the computations of a laminar partial-oxidation methane flame in which the WSGG and SLW models were used as the spectral models, in conjunction with the  $P_1$  approximation as one of three investigated RTE solvers. Pal et al. [160] investigated the performance of both the P<sub>1</sub> and P<sub>3</sub> RTE solvers, among other popular RTE solvers. Several advanced variations of the FSK model were tested. The problem considered in this study was Sandia Flame D, which was both unscaled and scaled by a factor of 4. It was found that, for optically thin flames (such as the Sandia Flame D without scaling), the P<sub>1</sub> approximation with gray (Planck-mean) absorption coefficients offered just as much accuracy as other high-fidelity nongray models and RTE solvers, but at a computational cost that is several orders of magnitude lower. For the flame scaled by a factor of 4, the P<sub>3</sub> solver coupled with the multi-group version of the FSK spectral model offered the best compromise between accuracy and computational efficiency. In [105], radiation inside an internal combustion engine was modeled using the P<sub>1</sub> approximation in conjunction with the wide-band-based step-wise gray model as well as the FSK model. The  $P_1$  solver coupled with the step-wise gray model was found to yield solutions within 10% accuracy of benchmark results at one-thirtieth of the computational cost of high-fidelity benchmark computations. Wang et al. [161,162] studied radiation in several different flames using the P<sub>1</sub> approximation in conjunction with the WSGG and FSK spectral models. Finally, in a comprehensive recent study, Ge et al. [163] explored P<sub>N</sub>-based RTE solvers all the way up to P<sub>7</sub> in addition to other solvers for the Sandia D flame scaled by a factor of 4. The FSCK model was used for all computations. Overall, it was found that the P<sub>3</sub> approximation provided the best compromise between accuracy and computational efficiency. Approximations higher than P<sub>3</sub> yielded diminishing returns in terms of accuracy at a much larger computational cost. Quantitative comparisons between the  $P_N$  solvers of various orders and other RTE solvers will be shown in a section to follow once the other solvers have been discussed.

#### 4.2. Discrete Ordinates ( $S_N$ Approximation) and Finite Angle Methods

In the discrete ordinates method (DOM), rather than analytically express the directional dependence of the radiation intensity, the angular space is discretized, analogous to

Energies 2023, 16, 4250 21 of 40

discretizing a spatial domain into a set of nodes. Hence, the discrete ordinates method is the angular equivalent of the finite-difference method in space. The angular discretization has to follow a set of rules such that rotational symmetry and other properties of the angular space are preserved. These issues are discussed in [1]. The DOM does not conserve radiation energy. Furthermore, it causes the streaking of the energy along the directions chosen for solving the RTE—a phenomenon referred to in the literature as a ray effect. The method also suffers from false scattering, a numerical artifact that manifests itself when the direction along which the RTE is solved is not aligned with the grid lines. In order to mitigate these shortcomings of the DOM, the so-called finite-volume method for radiation was proposed [164–167]. This method is analogous to the finite-volume method in space. Instead of solving the RTE along prescribed directions (angular nodes), the angular space is first split into a set of nonoverlapping solid angles analogous to control volumes in space. The RTE is first analytically integrated within each solid angle to develop a new RTE that represents radiation energy propagation over the entire solid angle rather than in discrete directions (as in the original DOM). This method guarantees the conservation of energy and significantly mitigates ray effects and false scattering. Since the method has no connection with finite volumes but, rather, uses finite solid angles, it was recently named, more logically, the finite angle method (FAM) [1]. Here, the FAM, instead of the DOM, is outlined since most computations of the RTE today employ FAM rather than DOM. Furthermore, all commercial CFD codes use FAM.

The development of the directional RTEs using FAM first involves integrating Equation (9) over control volumes (or cells) followed by its integration over finite solid angles. The finite solid angles are generally described by polar and azimuthal angles  $\theta$  and  $\psi$ , respectively, as shown in Figure 9, and written as

$$\Omega_{i} = \int_{\Delta\Omega_{i}} d\Omega = \int_{\theta_{i} - \Delta\theta_{i}/2}^{\theta_{i} + \Delta\theta_{i}/2} \int_{\psi_{i} - \Delta\psi_{i}/2}^{\psi_{i} + \Delta\psi_{i}/2} \sin\theta d\theta d\psi = 2\sin\theta_{i} \sin\left(\frac{\Delta\psi_{i}}{2}\right) \Delta\psi_{i}.$$
 (30)

Details of the derivation of the directional RTEs after spatial and angular integration are beyond the scope of this article, and may be found in Chapter 16 of [1]. The resulting directional RTEs are as follows:

$$\sum_{f=1}^{N_f} I_{\eta,i,f} \left( \mathbf{S}_i \cdot \hat{\mathbf{n}}_f \right) A_f = -\beta_{\eta,P} V_P I_{\eta,i,P} \Omega_i + \beta_{\eta,P} V_P S_{\eta,i,P} \Omega_i, \quad i = 1, 2, \dots, n,$$
 (31)

where the index i denotes directions (or solid angles) with a total of n directions. The summation on the left hand side of Equation (31) is over the faces, f, of the cell in question, P, with a total of  $N_f$  faces. The spectral intensity in the i-th direction and f-th face is denoted by  $I_{\eta,i,f}$ , while the same quantity at the cell-center is denoted by  $I_{\eta,i,P}$ .  $\hat{\mathbf{n}}_f$  and  $A_f$  are the outward-pointing surface normal and area of the f-th face.  $\beta_{\eta,P}$  and  $V_P$  denote the spectral extinction coefficient and volume of cell P, respectively. The quantity,  $\mathbf{S}_i$ , is given by

$$\mathbf{S}_{i} = \int_{\Omega_{i}} \hat{\mathbf{s}}_{i} d\Omega = \int_{\Delta\theta_{i} - \Delta\theta_{i}/2}^{\Delta\theta_{i} + \Delta\theta_{i}/2} \int_{\Delta\psi_{i} - \Delta\psi_{i}/2}^{\psi_{i} + \Delta\psi_{i}/2} (\sin\theta\cos\psi\hat{\mathbf{i}} + \sin\theta\sin\psi\hat{\mathbf{j}} + \cos\theta\hat{\mathbf{k}}) \sin\theta d\theta d\psi$$

$$= \left[ (\Delta\theta_{i} - \cos2\theta_{i}\sin\Delta\theta_{i})\cos\psi_{i}\sin\left(\frac{\Delta\psi_{i}}{2}\right) \right] \hat{\mathbf{i}}$$

$$+ \left[ (\Delta\theta_{i} - \cos2\theta_{i}\sin\Delta\theta_{i})\sin\psi_{i}\sin\left(\frac{\Delta\psi_{i}}{2}\right) \right] \hat{\mathbf{j}} + \sin2\theta_{i}\sin\Delta\theta_{i} \left(\frac{\Delta\psi_{i}}{2}\right) \hat{\mathbf{k}}. \tag{32}$$

Energies **2023**, 16, 4250 22 of 40

Finally, the source term of the directional RTEs (Equation (31)) is written as

$$S_{\eta,i,P} = \frac{\kappa_{\eta,P}}{\beta_{\eta,P}} I_{b\eta,P} + \frac{\sigma_{s\eta,P}}{4\pi\beta_{\eta,P}} \sum_{i=1}^{n} I_{\eta,j,P} \bar{\Phi}_{\eta,ij},$$
(33a)

$$\bar{\Phi}_{\eta,ij} = \frac{1}{\Omega_i} \int_{\Omega_i} \int_{\Omega_j} \Phi_{\eta}(\hat{\mathbf{s}}', \hat{\mathbf{s}}) d\Omega' d\Omega.$$
 (33b)

Prior to the solution of Equation (31), the face intensities must be replaced by cell-center intensities. The two most widely used schemes for this purpose are the *step scheme* (first-order upwind scheme) or the *diamond scheme* (second-order extrapolated central difference scheme), and a discussion of these schemes and others may be found elsewhere [1,168].

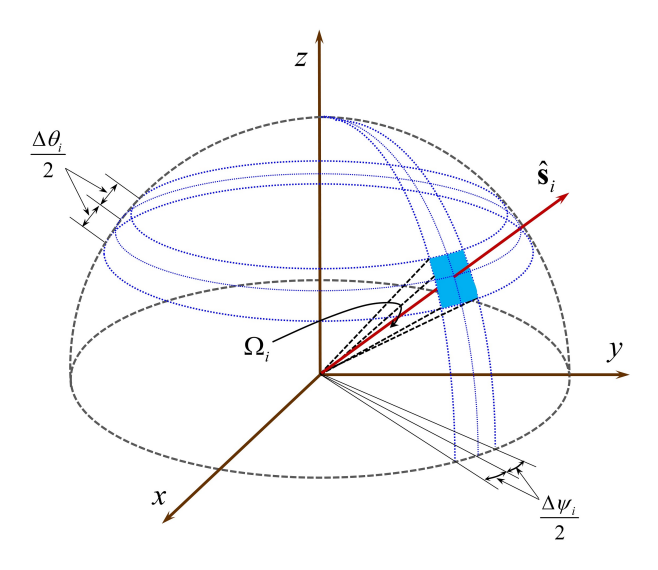


**Figure 9.** Finite solid angles used in the finite angle method and their representation in terms of polar and azimuthal angles.

The finite angle method, when applied to the boundary condition for the RTE, after some manipulation, yields the following relationship for all intensities leaving the boundary, i.e., for which  $\mathbf{S}_i \cdot \hat{\mathbf{n}}_w > 0$  [1]

$$I_{\eta,i,w} = \epsilon_{\eta,w} I_{b\eta w} + (1 - \epsilon_{\eta,w}) \frac{\sum\limits_{\mathbf{s}_{i} \cdot \hat{\mathbf{n}}_{w} < 0} I_{\eta,i,w} |\mathbf{S}_{i} \cdot \hat{\mathbf{n}}_{w}|}{\sum\limits_{\mathbf{s}_{i} \cdot \hat{\mathbf{n}}_{w} > 0} (\mathbf{S}_{i} \cdot \hat{\mathbf{n}}_{w})}, \tag{34}$$

where  $I_{\eta,i,w}$  is the diffuse spectral intensity leaving the boundary face w and  $\hat{\mathbf{n}}_w$  is the unit surface normal at w pointing out the boundary and into the computational domain. For intensities going into the boundary face w, i.e.,  $\mathbf{S}_i \cdot \hat{\mathbf{n}}_w < 0$ , using the step scheme, for instance, the face intensity may be replaced by the cell-center intensity:  $I_{\eta,i,w} = I_{\eta,i,P}$ . Equation (31) may now be solved and readily subject to the boundary conditions given by Equation (34). These equations represent a set of coupled linear algebraic equations—one set for each direction. Traditionally, they are solved in a segregated manner, i.e., one direction at a time in the sequence using standard iterative solvers. In the absence of scattering and reflective boundaries, these directional equation sets are not coupled. In the presence of strong scattering and/or strongly reflective boundaries, the coupling between directions may become strong, and the coupled solution of the full set of directional equations may be warranted to attain convergence, as demonstrated by Mathur and Murthy [169,170].

Both the DOM and the FAM have been extensively used for the computation of radiative transport in combustion environments [124,137,159,160,163,171–174]. In an early study, Mazumder and Modest [137] used the DOM with an  $S_4$  quadrature scheme and

Energies 2023, 16, 4250 23 of 40

the FSCK spectral model to simulate a gas turbine combustor with propane as the fuel. A gray model with Planck-mean absorption coefficients was also exercised, and showed a significantly lower temperature than that predicted by the FSCK model. In the past decade, with the growth in computational resources, Consalvi and co-workers [171–173] explored various RTE solvers and spectral models for the computation of laminar diffusion flames in axisymmetric computational domains. Both the standard DOM with T<sub>3</sub> quadrature and the FAM were explored, although no direct comparison between the RTE solvers was reported. In terms of spectral models, the FSCK and the statistical NBCK models for gas radiation were used in conjunction with both gray and nongray models for soot. Garten et al. [159] conducted computations with the standard DOM (one among three RTE solvers considered) paired with the WSGG and SLW models for the computation of radiation in a laminar methane-air partial oxidation flame. Pal et al. [160] conducted FAM calculations with two different angular grids:  $6 \times 2$  and  $16 \times 4$ . The accuracy of the coarser angular grid was found to be unacceptable. The finer angular grid yielded accurate solutions but at a relatively large computational cost. In [174], the standard DOM with the so-called  $L_2$ quadrature scheme was used to model the radiation transport in a 3D enclosure with combustion gases. To approximate facial intensities, the exponential scheme [175] was used, rather than the step or diamond schemes. The RTE solvers were paired with the WSGG spectral model. In [124], a DOM-based RTE solver with the  $S_4$  scheme and paired with the WSGG nongray model was coupled to an LES code to study compartment fires. The DOM was also extensively used by Selçuk and co-workers for solving the RTE in fluidized-bed combustors using the method of lines [132,176].

#### 4.3. Monte Carlo (MC) Method

The Monte Carlo (MC) method is a statistical method that has been traditionally used for, and found to be attractive for, solving differential equations of higher dimension. An example of such an equation is the PDF transport equation mentioned in Section 2.3.2, which is not only time- and physical-space-dependent, but also dependent on the composition space, comprising *N* species, and the enthalpy. Likewise, as mentioned earlier, the RTE has six independent variables, making it amenable for a solution using the MC method.

The MC method has a long history for the solution of the RTE (see Chapters 7 and 20 of [1] and Chapter 14 of [4]). A detailed discussion of the method as it pertains to the solution of the RTE is well beyond the scope of this article and may be found in [1,4]. In this method, statistical samples, representing photon bundles, are sampled from the probability density functions constructed from the basic laws of radiation. The photon bundles are then allowed to interact with each other and with the medium, and the interactions are governed by the path they travel and the spectral extinction coefficient encountered along the path. Quantities of interest, such as the heat flux or its divergence (radiation source) are computed by locally tallying the statistical samples. The statistical error in the solution depends on the number of samples used in the computation.

In grid-based deterministic methods, the solution accuracy is primarily dependent on the grid used in each dimension, such as the physical grid spacing, the number of directions used in the case of DOM or FAM, and the number of spectral intervals used for nongray media. The solution may be grid-independent in one dimension but not in others and reduction in the overall error in solution requires resolution in multiple dimensions, resulting in the super-linear scaling of the computational cost with the number of dimensions in the problem. In contrast, in the MC method, the statistical error scales as  $N_s^{-1/2}$ , where  $N_s$  is the total number of samples [1] used in the computation. It does not matter how many dimensions the problem has. Of course, if the number of dimensions is large, the number of samples that must be used to arrive at an accurate result must also be, correspondingly, larger. However, there is no direct quantifiable relationship between the number of dimensions, the accuracy of the solution, and the computational cost.

Over the past three decades, tremendous advances have been made in developing and applying the MC method to radiation transport in combustion environments [158,160,163,177–188].

Energies 2023, 16, 4250 24 of 40

Most notably, Modest and coworkers have developed MC methods that particularly address the strongly oscillating behavior (line stricture) of the absorption coefficients of combustion gases, resulting in the so-called *line-by-line photon Monte Carlo method* or LBL-PMC [177,180]. This method has, since its inception, been applied to generate benchmark results for turbulent flames [160,163]. The sampling techniques in the MC method were also extended to enable the use of the method in conjunction with full-spectrum *k*-distributions [179]. Random number databases that allow the efficient sampling of the photon bundles were also developed and disseminated [189,190]. The MC method has also been extended to include multiphase media, such as combustion environments with solid particles or liquid droplets [182,183,191].

Traditionally, MC methods employ so-called *pseudo* random numbers. It has been found that semi-deterministic low-discrepancy sequences, such as the Halton sequence or the Sobol sequence, which result in so-called *quasi*-random numbers, yield better statistical convergence. The quasi-MC (QMC) method was originally used for surface-to-surface radiative transfer applications [192–194], and has now found its way into modeling radiative transfer in combustion environments [186,188,195]. The rate of convergence—defined by how quickly the statistical error decreases with the number of photons used in the simulation—for QMC is faster than PMC, as shown in Figure 10. Palluotto et al. [195] showed that, with appropriate randomization, QMC can possibly achieve an even faster convergence rate. Farmer and Roy [186] compared the figure of merit (FoM) of QMC and PMC. FoM is defined from the root-mean-squared error,  $\epsilon$ , and the computational time, t, such that a higher FoM is indicative of a more efficient method:

$$FoM = \frac{1}{\epsilon^2 t}.$$
 (35)

In their comparison, Farmer and Roy [186] found the FoM of QMC to be several times higher than that of PMC in several flame configurations, including a high-pressure flame and a pool fire. For example, Figure 11 shows the error in the absorbed radiation energy field obtained from PMC and QMC for a pool fire calculated using  $4 \times 10^8$  photon bundles. The error is calculated with reference to a benchmark solution calculated using  $5 \times 10^9$  photon bundles. The level of error from the benchmark is visibly smaller in the QMC solution than in the PMC solution. While QMC holds the promise of making MC methods computationally very attractive for large-scale simulations, it has also been reported that a strongly scattering medium or reflective boundaries may lead to some decrease in the efficiency of QMC [186,188].

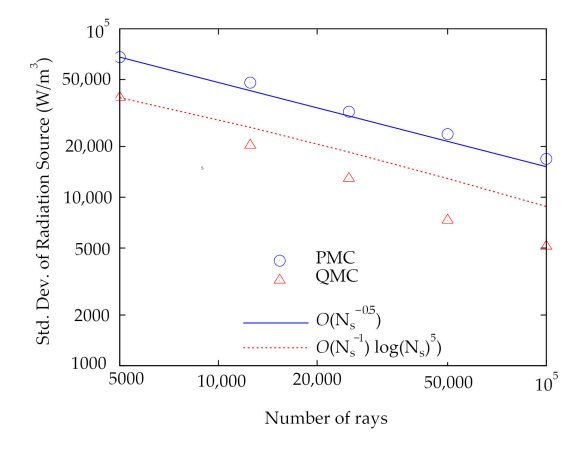


**Figure 10.** Comparison of the rate of convergence of QMC and PMC for the computation of a radiative source in a one-dimensional plane-parallel media; adopted from [186].

Energies **2023**, 16, 4250 25 of 40

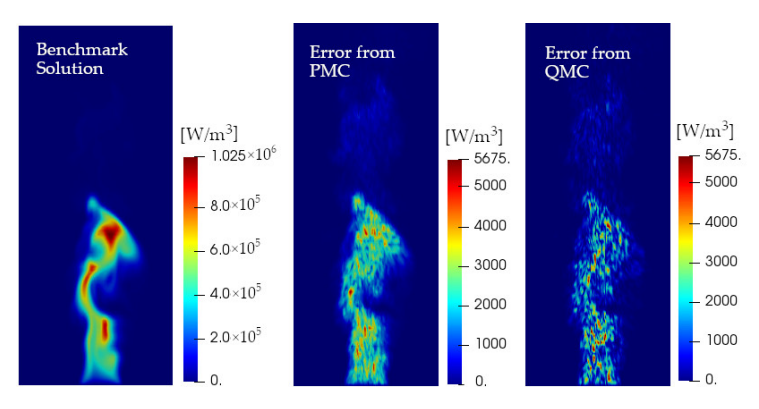


**Figure 11.** Comparison of the error from the benchmark solution in the absorbed radiation energy field obtained from PMC and QMC using the same number of photon bundles in a pool fire; adopted from [186].

## 4.4. Hybrid Methods

As discussed earlier, the two most popular deterministic methods for the solution of the RTE have some shortcomings. The  $P_1$  approximation is not particularly suited to scenarios in which an optically thin medium is bounded by hot and cold walls. The next order,  $P_3$ , which can address stronger anisotropy in the intensity, is not particularly easy to implement (the resulting equations are coupled and have cross-derivatives). When it comes to the DOM or the FAM, while the method is trivial to extend to higher orders to improve accuracy, the extension comes at an increased computational cost. Given that the lowest-order versions of DOM or FAM already require a solution of more than 6–8 directional RTEs, and the computational cost quickly becomes appreciable, especially for nongray combustion media. In addition, DOM and to a lesser extent, FAM, suffer from ray effects and false scattering. Its convergence has also been found to be poor for optically thick scenarios [169,170].

A number of hybrid methods have been developed over the past three decades in an effort to address the shortcomings of these two core RTE solvers. Here, a handful of these that have been specifically applied to nongray combustion scenarios is discussed. One such method is the so-called modified differential approximation (MDA) [196]. In this method, the intensity is split into a "medium" and a "wall" component. The medium component, by virtue of being fairly isotropic, can be treated accurately using the  $P_1$  approximation. The wall component, on the other hand, is strongly anisotropic and is generally treated using a view factor-based approach [196,197]. Garten et al. [159] conducted laminar methane-air flame computations in which the WSGG and SLW models were used in conjunction with the MDA. The MDA combined with the SLW model yielded very accurate solutions. However, like previous studies [197], it was concluded that computing the wall component of the intensity using a view factor-based approach in the MDA is computationally expensive. Sankar and Mazumder [198] suggested using FAM for the wall component, which not only improved the computational efficiency of the method, but also made it amenable to computations in large-scale complex geometries. Another hybrid approach exploits the spectral nature of the RTE in combustion applications for hybridizing. Yadav et al. [199] hybridized the P<sub>1</sub> approximation with DOM using the WSGG spectral model. They used the P<sub>1</sub> approximation for two out of the four gray gases and found a 30% gain in computational efficiency without significant loss in accuracy. Sun and Zhang [200] hybridized P<sub>1</sub> and FAM for the SLW model with 11 gray gases and found a 32% reduction in computational time and a 3% error (compared to FAM for all gases) in the heat source when 4 out of the 11 gases were solved using P<sub>1</sub>. A similar hybrid approach was recently used by Sun et al. [201] for flame calculations and implemented within the open source CFD code OpenFOAM. Jajal and Mazumder [202,203] considered a NB-based step-wise gray model (based on the EM2C database [109,110]) for a combustion gas mixture, and developed a hybrid solver in which the P<sub>1</sub> approximation was used for some of the bands, while the FAM was used for the

Energies **2023**, 16, 4250 26 of 40

others. Two different approaches were used for demarcation. In the so-called *cutoff approach*, a prescribed cutoff optical thickness was used to demarcate between  $P_1$  and FAM bands. In the so-called *filter approach*, an optical thickness window was used. Within this optical window, the FAM was used, while  $P_1$  was used outside the window. Figure 12 shows the sample results for a nonisothermal 3D enclosure filled with a combustion gas mixture of  $CO_2$  and  $H_2O$ . The hybrid filter approach with an optical thickness filter of 0.5–5 appears to quite accurately predict the radiative source (Part a), but fails to accurately predict the radiative heat flux at one of the enclosure walls (Part b). In contrast, both quantities are quite accurately predicted by the hybrid cutoff approach with an optical thickness cutoff of 0.5. However, the cutoff approach uses  $P_1$  only for 69 out of the 349 bands, and provides only 21% savings in computational time. In contrast, the filter approach uses  $P_1$  for 280 out of the 349 bands, and results in computational savings of 55%. The MC method has also been hybridized with FAM by Sun et al. [204], wherein the MC method was only used to sample the wavenumbers for which the RTEs are to be solved. The RTEs for these sampled wavenumbers were then deterministically solved using FAM.

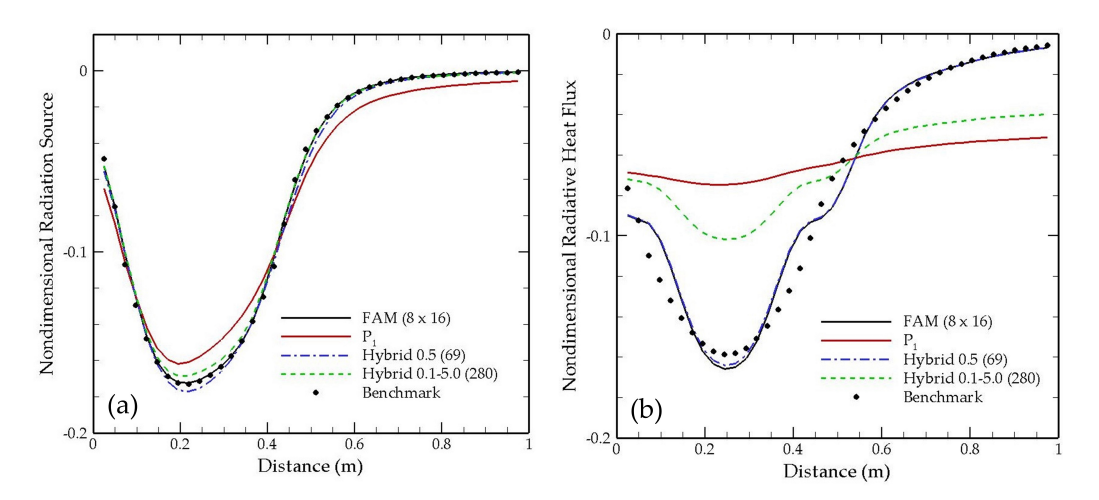


**Figure 12.** Comparison of the accuracy of the  $P_1$  approximation, the FAM, and the hybrid solver: (a) radiative heat source; and (b) radiative heat flux; adopted from [203]. For the hybrid solver, the number of  $P_1$  bands are shown in parenthesis.

## 4.5. Comparison of RTE Solvers

Although numerous studies have focused on the solution of the RTE in combustion environments, and several others have compared various nongray models, very few studies have actually quantitatively compared the various RTE solvers. Table 1 provides a brief summary of some studies that have attempted to do so, particularly within the past three decades. Other than the RTE solvers mentioned in Table 1, the Zonal method [1,4] has also been used on a handful of occasions. It is clear that the  $P_N$  method (in particular,  $P_1$ ), the DOM, and the FAM are the three most popular deterministic methods. The PMC has also been used, but only by Modest and coworkers.

**Table 1.** Summary of studies dedicated to the assessment of RTE solvers in combustion environments.

	• · · · · · · · · · · · · · · · · · · ·	
Topic	References	RTE Solver Studied

Topic	References	RTE Solver Studied
Laminar flame	[158,159,171–173,187,205]	PMC, DOM, FAM, P <sub>1</sub> , MDA, SP <sub>3</sub> , SP <sub>5</sub>
Laboratory-scale turbulent flame	[3,160,163,206]	PMC, DOM, FAM, P <sub>1</sub> –P <sub>7</sub>
Turbulent combustors, furnaces, and engines	[105,137,174,207–211]	PMC, P <sub>1</sub> , DOM, FAM
Other combustion applications	[106,137,199,200,203,212]	PMC, DOM, FAM, P <sub>1</sub> , hybrid

Energies **2023**, 16, 4250 27 of 40

RTE solvers were compared in the context of laminar flame calculations by a few researchers. Consalvi and co-workers [171–173] explored the standard DOM with the T<sub>3</sub> quadrature, as well as the FAM, in conjunction with the FSCK and the statistical NBCK models. For the FAM calculations, angular discretizations such as  $36 \times 48$  or  $24 \times 32$ were used, but no direct comparison was made between the various angular resolutions. Cai et al. [158] studied laminar hydrogen-air diffusion flames under atmospheric and highpressure conditions. Benchmark RTE solutions were obtained using LBL-PMC. The RTE was solved using the P<sub>1</sub>, SP<sub>3</sub>, and SP<sub>5</sub> approximations. The FSCK model was used as the nongray model for the deterministic solvers. The results show that neither SP<sub>3</sub> nor SP<sub>5</sub> offered noticeably better accuracy over P<sub>1</sub>, except when the pressure was raised significantly. The computational costs of the three deterministic solvers were found to be comparable. On the other hand, the LBL-PMC calculations required approximately twice as much computational time as the FSCK-based deterministic solvers. In the deterministic solvers paired with FSCK, the majority of the computational time was spent in retrieving data from the k-distribution database, and the actual solution time of the RTE was found to be relatively small. In the PMC method, in contrast, most of the computational time was spent sampling and tracing photon bundles. So-called time blending [15,158,163] was used in the PMC code, wherein information from the tracing photon bundles at previous iterations was used to reduce the number of bundles that need to be traced at the current iteration while still maintaining the desired statistical accuracy. With this strategy, 100 times fewer bundles needed to be traced per iteration. Time blending is almost mandatory to keep PMC tractable for such combustion calculations. With advances in assembling and using k-distributions [147], including machine learning [150], the computational overhead of the FSCK method can be reduced even further. Garten et al. [159] compared the P<sub>1</sub> approximation, the MDA, and the DOM for the solution of the RTE in a laminar methane partial oxidation flame. The MDA provided the best compromise between accuracy and efficiency, but only if the walls had isothermal boundary conditions, the allowing computation of the wall component only once.

The modeling of radiation in turbulent combustion environments is challenging for the reasons discussed in Sections 2.2 and 2.3. In consideration of these challenges, two approaches have been adopted to assess radiation models for combustion applications. The first approach is one where the temperature and concentration fields are first computed (either at steady state or at a particular instance of time) without radiation using a method of choice, e.g., RANS, LES, PDF, etc. These computed fields then serve as inputs into a radiation module that computes the radiative source and heat flux. In other words, there is only a one-way transfer of information, and the radiation field is a byproduct of the prescribed or frozen temperature and concentration fields. The second approach is one where the radiation source is fed back into the energy equation, and the temperature and concentration fields are iteratively recomputed, i.e., full two-way coupling. The vast majority of assessments of RTE solvers and spectral models fall into the first category. Pal et al. [160] comparatively assessed the FAM, P<sub>1</sub> and P<sub>3</sub> solvers paired with sophisticated nongray models, such as the FSK and its more sophisticated multiscale multigroup variants. Sandia Flame D, both unscaled and scaled by a factor of 4, was used for these investigations. Benchmark results for the radiative source with freezing temperature and concentration fields were obtained using the LBL-PMC solver. It was found that for optically thin flames, e.g., the Sandia Flame D without scaling, the  $P_1$  solver coupled with a gray (Planck-mean) model offers almost the same accuracy as the benchmark solution, but at a computational cost that is several orders of magnitude lower. For optically thicker flames, the P<sub>3</sub> solver coupled with the multiscale FSK model offered the best accuracy, while being computationally comparable in cost to the LBL-PMC solver for stationary (steady-state) calculations in which time blending was effectively used for LBL-PMC. For transient calculations, wherein time blending is not as effective for LBL-PMC, the highest-fidelity deterministic solver outperformed LBL-PMC by more than an order of magnitude in terms of computational efficiency. Both Orbegoso et al. [206] and Wang et al. [161] studied the same soot-laden

Energies **2023**, 16, 4250 28 of 40

turbulent diffusion flame [162]. In [206], DOM was paired with the WSGG model, while in [161], P<sub>1</sub> was paired with the FSK model. In both studies, two-way coupling was included. In some cases, the WSGG results were found to better match experimental data than the FSK model. However, since these studies were conducted by different groups with different RTE and turbulent reacting flow solvers, it is not clear where the discrepancies stem from. In a recent comprehensive study, Ge et al. [163] compared  $P_N$  and FAM solvers of various orders/angular resolutions, coupled to the latest version of the FSCK model for the computation of Sandia Flame D scaled by a factor of 4. Both the frozen field as well as the two-way coupled computations were conducted. Once again, benchmark results were obtained using LBL-PMC. For frozen-field computations, the radiation source predicted by various RTE solvers is shown in Figure 13. The  $P_N$  solvers consistently overpredict the radiation source, with P<sub>1</sub> having the worst accuracy. The improvement in accuracy from P<sub>1</sub> to P<sub>3</sub> is fairly drastic, with diminishing returns from subsequent increase in the order. Hence, it may be concluded that P<sub>3</sub> offers a reasonable compromise between the accuracy and computational efficiency. Overall, the FAM solvers predict the radiation sources with better accuracy compared to the  $P_N$  solvers, with even the lowest-resolution FAM, i.e.,  $2 \times 4$ , yielding surprisingly accurate results.

For two-way coupled solutions, since local conditions change with the radiation model being used, rather than considering local radiation sources, conventional practice is to examine quantities that are measurable and are of engineering interest, such as local temperature and NO concentrations. Figure 14 shows the radial distributions of temperature and NO mass fractions. For temperature predictions, no significant difference is noted between the various  $P_N$  solvers. Likewise, minor differences are observed between the various FAM solvers. The  $P_N$  solvers slightly underpredict the mean temperature, which manifests itself in a significant underprediction of the mean NO mass fractions. Overall, the FAM solvers, with the exception of the lowest-resolution  $2\times 4$ , accurately predict both temperature and NO concentrations, especially considering the complexity of such calculations.

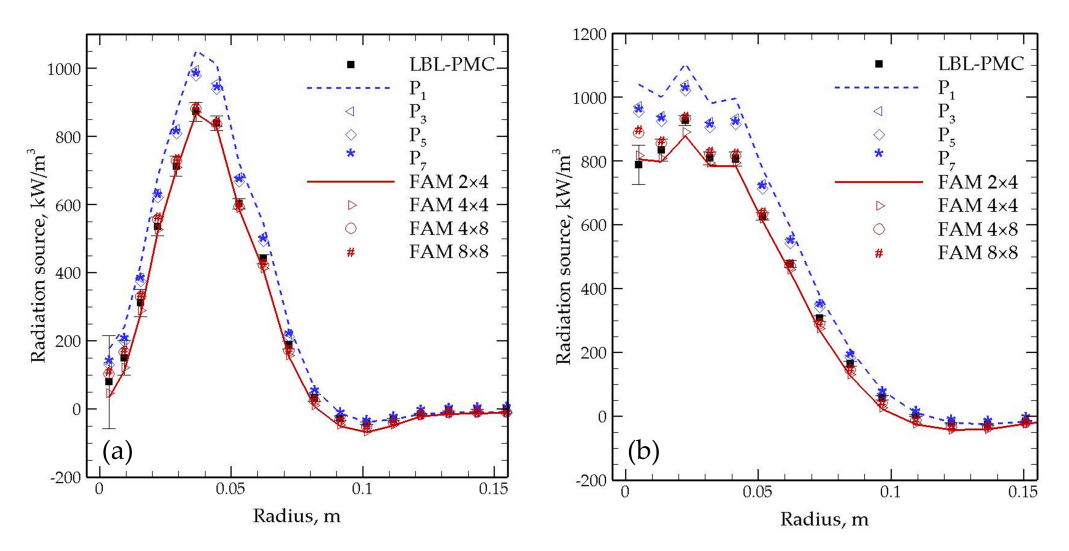


**Figure 13.** The radial distribution of the radiation source predicted by various RTE solvers for the computation of the Sandia Flame D (turbulent jet flame) scaled up by a factor of 4 using prescribed (frozen) temperature and concentration fields: (a) 30 jet diameters from inlet; and (b) 45 jet diameters from the inlet; adopted by [163].

Energies 2023, 16, 4250 29 of 40

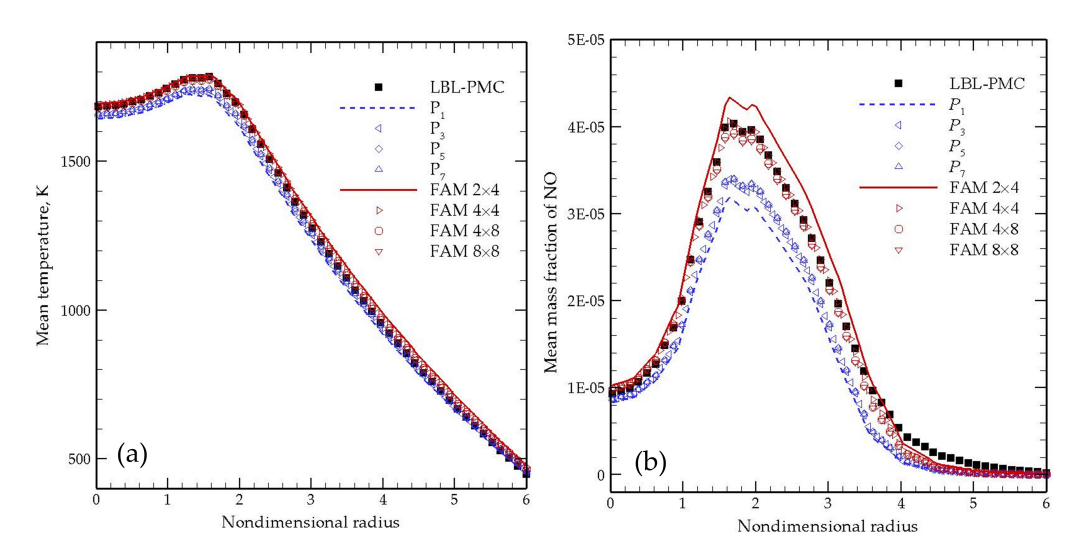


**Figure 14.** The radial distribution of temperature and nitric oxide (NO) mass fractions at 45 jet diameters from the inlet predicted by various RTE solvers for the computation of the Sandia Flame D (turbulent jet flame) scaled up by a factor of 4 with full coupling: (a) temperature; and (b) nitric oxide mass fraction; adopted from [163].

While the FAM solvers appear to slightly outperform the  $P_N$  solvers, especially for fully coupled solutions, the increased accuracy is also accompanied by an increased computational cost. Ge et al. [163] separately recorded the time taken to solve the RTE for fully coupled solutions. When compared to the time taken to solve the problem without radiation,  $P_1$  required 18% more time,  $P_3$  required 28% more time, while  $P_7$  required 100% more time. Similarly, FAM 2  $\times$  4 required 35% more time, FAM 4  $\times$  4 required 46% more time, while FAM 8  $\times$  8 required 117% more time. In other words, the lowest-resolution FAM solver (2  $\times$  4) required approximately twice as much time as the lowest-order  $P_N$  solver ( $P_1$ ). The next higher resolution FAM (4  $\times$  4) requires approximately 1.64-fold the amount of time required by  $P_3$ . Based on the results of this single study, it may be concluded that, if only the mean temperature is of interest, then the  $P_1$  solver may suffice. However, if interested in predicting pollutants such as NO, a slightly more computationally expensive RTE solver, such as FAM 4  $\times$  4 or  $P_3$ , may be the most desirable option.

To summarize, a survey of the literature suggests that the two most popular solvers for solving the RTE in combustion environments are the DOM (and its more popular variant, the FAM), and the  $P_1$  approximation. The DOM (and FAM) is easily extendable to a higher order, making it attractive. Although higher-order  $P_N$  solvers appear to be equally promising from an accuracy standpoint, the extension of  $P_1$  to higher orders is nontrivial and requires significant additional code development. Of the two methods, the DOM is computationally more expensive, especially for 3D calculations. Hybrid methods that hybridize these two popular solvers appear to show promise. Beyond these two methods, the photon Monte Carlo (PMC) method continues to be popular, particularly for generating benchmark solutions for steady-state (or statistically stationary in the case of turbulent) calculations with full two-way coupling.

#### 5. Concluding Remarks and Future Perspectives

Modeling thermal radiation in combustion environments is challenging. First, the inclusion of radiation makes the overall energy conservation equation strongly nonlinear. Secondly, the radiative transfer equation or RTE, which is the cornerstone of modeling radiation in any participating (or nontransparent) medium, is a five-dimensional integro-differential equation with a wavenumber (or wavelength) as an additional parameter, i.e., the RTE needs to be solved for multiple wavenumbers. Thirdly, the absorption coefficient of most molecular gases and, to some extent, the scattering coefficient of particulates and droplets, is characterized by wild oscillations with the wavenumber, implying that the

Energies **2023**, 16, 4250 30 of 40

RTE needs to be solved numerous times to accurately compute the contributions of all wavenumbers to the net heat flux or its divergence (the radiation source in the energy conservation equation). To complicate matters further, most practical combustion applications involve turbulent flow fields. Turbulence causes all state variables (temperature, pressure, enthalpy, concentrations) to fluctuate at length and time scales that span several orders of magnitude. Since radiative properties depend on these quantities, the radiation intensity, which is dictated by radiative properties, also fluctuates. This results in so-called turbulence—radiation interactions (TRIs) in addition to turbulence—chemistry interactions, whose modeling already poses significant challenges. These, and others, constitute some of the reasons why radiation has largely been neglected or addressed using rudimentary models for decades in combustion computations.

Over the past three decades, significant progress has been made in modeling thermal radiation transport in combustion systems. Broadly, they may be categorized into advancements in four major fronts: (1) radiative property compilation; (2) spectral model development; (3) RTE solver development; and (4) the treatment of TRIs.

Radiative property compilation. Until 1990, most nongray radiation calculations in combustion systems relied on either wide-band or narrow-band data for emissivity or transmissivity, mostly measured experimentally and then fitted to empirical correlations [107,108]. Consequently, the accuracy of these data is somewhat limited. Furthermore, as mentioned earlier, such data are not for the raw spectral absorption coefficients of the various gases and, therefore, cannot be used within the framework of the general RTE. With the advent of high-resolution spectroscopic databases, such as HITRAN, HITEMP, CDSD, and others, extracting (computing) the raw spectral absorption coefficients of combustion gases over a wide range of temperature, pressure, and concentrations, is now possible. While heat transfer experiments have their usefulness in validating the computed (from spectroscopic databases) radiative properties, they cannot provide data at a resolution that these spectroscopic databases provide. Consequently, the development of state-of-the-art spectral models over the past three decades has heavily relied on raw spectral absorption coefficients computed from spectroscopic databases. With the advent of high-performance computing, it is now also possible to compute spectral scattering coefficients and the scattering phase-functions of particulates and droplets either by solving the foundational Maxwell's equations of electromagnetic wave propagation, or by using scattering theories, such as the Mie theory or Rayleigh–Debye–Gans theory (see Chapter 11 of [1]). The determination of the spectral optical properties of soot remains a challenge due to the complexity of soot processes and an incomplete understanding of soot composition and morphology. However, recent explorations in ab initio soot modeling [213–216] may provide a promising outlook for detailed soot optical property modeling. One major challenge facing the research community is the ability to keep up with newer versions of the spectroscopic databases. Computing the absorption coefficient from the data contained in these databases is not a trivial task, and takes considerable time and effort to compute from the ground up. With the explosion of machine learning techniques, perhaps, it may be possible to consolidate newer information into older databases in an "additive" manner.

**Spectral model development.** As highlighted in Section 3.4, two of the most popular and accurate spectral models for combustion gases in use today are the SLW and FSK models. Developed in the 1990s, both models have witnessed dramatic refinements making them not only more accurate, but also more amenable to the large-scale computations of combustion systems. A number of research groups, both within the United States and in Europe, are actively engaged in further refining these two models and extending them to cover new applications, such as remote sensing [217], and radiation transport in condensed matter [218] and liquid fuels [143]. While both models are accurate and computationally efficient, both require extensive databases. Over the past two decades, databases (of either k-distributions or absorption cross-sections) and codes to compile these databases have been publicly published and disseminated, as mentioned in Section 3.1. Currently, extracting data from these databases appears to be a major computational bottleneck in using these

Energies **2023**, 16, 4250 31 of 40

methods rather than the solution of the RTE itself. In recent years, machine-learning-based algorithms to extract data from these databases have been developed [150,219]. Further progress on this front is expected to make computations using these models even more efficient. As in the case of the raw spectral absorption coefficient data (see previous paragraph), databases containing k-distributions and absorption cross-sections will also require updates alongside updates in the underlying spectroscopic databases and, currently, there appears to be no convenient or efficient method to do so.

RTE solver development. Advances in CFD over the past three decades have also been accompanied by advances in RTE solution techniques. While the P<sub>1</sub> approximation and the DOM (or FAM) were already in existence in the mid-1990s, they have been tremendously improved and extended. Most notably, both methods have now been adopted and routinely used for unstructured mesh topologies [168,174,197,198,203,204,220–223], although not always for combustion applications. Most commercial CFD codes and public-domain codes, such as OpenFOAM, are now equipped with a parallel unstructured FAM-based RTE solver. In comparison to P<sub>1</sub> and DOM/FAM, limited progress has been made in the development of  $P_3$  and other higher-order  $P_N$  solvers. Except for the work by Ravishankar et al. [224], who demonstrated the P<sub>3</sub> solver for unstructured meshes in both 2D and 3D geometries, most of the developments have stemmed out of the work of modest and coworkers [1,157]. Although extensively used by them for the solution of the RTE in combustion environments,  $P_3$  and other higher-order  $P_N$  solvers do not appear to have been used in 3D geometries for combustion applications. Hence, there is a need to extend the P<sub>3</sub> and other higherorder  $P_N$  solvers to 3D combustion calculations to truly assess their scaling behavior for large-scale computations.

Significant progress has also been achieved on the MC method. In particular, the lineby-line-based photon MC (LBL-PMC) technique developed by Modest and coworkers [1,180] represents a major breakthrough, whereby the LBL accuracy can now be attained in actual combustion applications (within statistical error bars), such as flames and combustors. While the statistical errors in MC methods, in principle, are unrelated to any grid, in practice, MC-based RTE solvers are coupled to an underlying deterministic solver for the overall energy equation. The error in the computed local radiative source depends on how many samples are available within the local cell (spatial bin); the smaller the cell, the fewer the number of samples, and the larger the *local* statistical error. In other words, while mesh refinement increases the accuracy of the deterministic solver for the energy equation, it has an adverse effect on the local statistical errors incurred within the MC algorithm. Using MC methods for problems with a large mesh count therefore requires an impractically large number of statistical samples with no guarantee that the resulting local statistical errors will be small. This may be the reason why the PMC-LBL method has not been applied to 3D problems with a relatively large mesh count. Several variance reduction techniques have also been explored to improve the solution accuracy and/or improve the statistical convergence. These include importance sampling, reciprocity MC, deviational MC, and QMC, among others. A detailed discussion of all of these techniques is beyond the scope of this article and may be found elsewhere [1,4,225]. It is worthwhile to note that only a few of these techniques have been applied to nongray radiative transfer in combustion environments. Further research is warranted to adapt these techniques to MC calculations in nongray combustion media.

Treatment of turbulence–radiation interactions (TRIs). Since most practical combustion applications involve turbulent flows, and since TRIs have been shown to publicly augment (often by more than 50%) heat loss from flames and fires (see Section 2.3 above and Section 22.4 of [1]), significant research has been dedicated to the modeling of TRIs in combustion environments. Research has shown that so-called *emission TRIs* are the dominant type of TRI. *Absorption TRIs*, on the other hand, have been found to be negligible in most flames including soot-laden luminous flames, but could be significant for large pool fires. Consequently, the vast majority of the research has been dedicated towards the refinement of models to address emission TRIs. With the LES of turbulent reacting

Energies **2023**, 16, 4250 32 of 40

flows gathering impetus, and with the development of advanced spectral models and RTE solvers, such as FSK and SLW paired with either FAM or  $P_N$  or LBL-PMC, it is now possible to model both emission and absorption TRIs with a reasonable level of confidence. The modeling of absorption TRIs, which is significantly more challenging than the modeling of emission TRIs, requires further attention and progress, especially with renewed interest in the high-fidelity modeling of wildfires.

Over the past decade, computer hardware and architectures have witnessed a dramatic overhaul and improvements in speed. From a strictly computer science standpoint, a limited number of studies have been reported to use the advanced parallel computing paradigms for the solution of the RTE. Modern hardware, such as graphical processing units (GPUs), as well as domain-specific languages that enable heterogenous parallelization, are being used extensively for the automatic generation and optimal execution of high-performance codes in other disciplines [226–229]. It is incumbent upon the developers of RTE solvers to adopt and apply these emerging resources and techniques so that radiation calculations in combustion environments can be scaled up to practical 3D combustors with a large mesh count.

**Author Contributions:** S.M.; writing—original draft preparation, S.P.R.; writing—review and editing. All authors have read and agreed to the published version of the manuscript.

**Funding:** Some of the material presented in this paper is based upon work supported by the National Science Foundation under Grant No. 2144290. Any opinions, findings, and conclusions or recommendations expressed in this material are those of the author(s) and do not necessarily reflect the views of the National Science Foundation.

**Data Availability Statement:** No new data were created or analyzed in this study. Data sharing is not applicable to this article.

**Acknowledgments:** Michael F. Modest is acknowledged for providing a Fortran code for the calculation of the spectral absorption coefficient of molecular gases from HITRAN/HITEMP, and for sharing the data used for Figure 4. Nehal Jajal is acknowledged for contributing to Figure 12. Wenjun Ge is acknowledged for sharing the data for Figures 13 and 14.

Conflicts of Interest: The authors declare no conflict of interest.

## Abbreviations

The following abbreviations are used in this manuscript:

CFD Computational Fluid Dynamics
DNS Direct Numerical Simulation
DOM Discrete Ordinates Method
FAM Finite Angle Method
FSK Full-Spectrum k-distribution

FSCK Full-Spectrum Correlated k-distribution

LBL Line-by-Line

LES Large Eddy Simulation

MC Monte Carlo NB Narrow Band

PDE Partial Differential Equation PDF Probability Density Function

PMC Photon Monte Carlo QMC Quasi-Monte Carlo

RANS Reynolds-Averaged Navier–Stokes RTE Radiative Transfer Equation

SLW Spectral Line-Weighted

TRI Turbulence–Radiation Interaction WSGG Weighted-Sum-of-Gray-Gases

WB Wide Band

Energies **2023**, 16, 4250 33 of 40

#### References

- 1. Modest, M.F.; Mazumder, S. Radiative Heat Transfer, 4th ed.; Academic Press: New York, NY, USA, 2021.
- 2. Modest, M.F.; Haworth, D.C. Radiative Heat Transfer in Turbulent Combustion Systems: Theory and Applications; Springer: Berlin/Heidelberg, Germany, 2016.
- 3. Modest, M.F. Radiative Heat Transfer in Turbulent Combustion 2021 Max Jakob Memorial Award Paper. *ASME J. Heat Mass Transf.* 2023, 145, 073101. [CrossRef]
- 4. Howell, J.R.; Mengüç, M.P.; Daun, K.J.; Siegel, R. Thermal Radiation Heat Transfer, 7th ed.; CRC Press: Boca Raton, FL, USA, 2021.
- 5. Mazumder, S. Numerical Study of Chemically Reactive Turbulent Flows with Radiative Heat Transfer. Ph.D. Thesis, The Pennsylvania State University, State College, PA, USA, 1997.
- 6. Modest, M.F. Multiscale Modeling of Turbulence, Radiation, and Combustion Interactions in Turbulent Flames. *Int. J. Multiscale Comput. Eng.* **2005**, *3*, 85–106. [CrossRef]
- 7. Modest, M.F., Radiative Heat Transfer Models for High-Temperature Combustion Gases. In *Annual Review of Heat Transfer*; Chen, G., Ed.; Begell Publishing: Danbury, CT, USA, 2005; Volume 14, Chapter I.2, pp. 23–47.
- 8. Mazumder, S.; Modest, M.F. A PDF Approach to Modeling Turbulence–Radiation Interactions in Nonluminous Flames. *Int. J. Heat Mass Transf.* **1999**, 42, 971–991. [CrossRef]
- 9. Coelho, P.J. Numerical simulation of the interaction between turbulence and radiation in reactive flows. *Prog. Energy Combust. Sci.* **2007**, 33, 311–383. [CrossRef]
- 10. Bird, R.B.; Stewart, W.E.; Lightfoot, E.N. Transport Phenomena, 2nd ed.; John Wiley & Sons, Inc.: New York, NY, USA, 2007.
- 11. Whitaker, S. Fundamental Principles of Heat Transfer, 1st ed.; Pergamon Press: New York, NY, USA, 1977.
- 12. Fox, R.O. Computational Models for Turbulent Reacting Flows; Cambridge University Press: Cambridge, UK, 2003.
- 13. Kumar, A.; Mazumder, S. Assessment of Various Diffusion Models for the Prediction of Heterogeneous Combustion in Monolith Tubes. *Comput. Chem. Eng.* **2008**, *32*, 1482–1493. [CrossRef]
- 14. Kumar, A.; Mazumder, S. Coupled Solution of the Species Conservation Equations Using Unstructured Finite-Volume Method. *Int. J. Numer. Methods Fluids* **2010**, *64*, 409–442. [CrossRef]
- 15. Wang, A.; Modest, M.F.; Haworth, D.C.; Wang, L. Monte Carlo Simulation of Radiative Heat Transfer and Turbulence Interactions in Methane/Air Jet Flames. *J. Quant. Spectrosc. Radiat. Transf.* **2008**, *109*, 269–279. [CrossRef]
- 16. Pope, S.B. Turbulent Flows; Cambridge University Press: Cambridge, UK, 2000.
- 17. Wilcox, D.C. Turbulent Modeling for CFD, 3rd ed.; DCW Industries: La Canada, CA, USA, 2006.
- 18. Pope, S.B. PDF Methods for Turbulent Reactive Flows. Prog. Energy Combust. Sci. 1985, 11, 119–192. [CrossRef]
- 19. Pope, S.B. PDF/Monte Carlo Methods for Turbulent Combustion and Their Implementation on Parallel Computers. In *Turbulence and Molecular Processes in Combustion*; Takeno, T., Ed.; Elsevier Science Publisher: Amsterdam, The Netherlands, 1993; pp. 51–62.
- 20. Cox, G. On Radiant Heat Transfer from Turbulent Flames. Combust. Sci. Technol. 1977, 17, 75–78. [CrossRef]
- 21. Mazumder, S.; Modest, M.F. Turbulence–Radiation Interactions in Nonreactive Flow of Combustion Gases. *ASME J. Heat Transf.* **1999**, 121, 726–729. [CrossRef]
- 22. Gupta, A.; Modest, M.F.; Haworth, D.C. Large-Eddy Simulation of Turbulence–Radiation Interactions in a Turbulent Planar Channel Flow. *ASME J. Heat Transf.* **2009**, *131*, 061704. [CrossRef]
- 23. Coelho, P.J. A theoretical analysis of the influence of turbulence on radiative emission in turbulent diffusion flames of methane. *Combust. Flame* **2013**, *160*, 610–617. [CrossRef]
- 24. Fraga, G.C.; Coelho, P.J.; França, F.H.R. Assessing individual time-averaged emission and absorption correlations for large-scale turbulent pool fires. *Int. J. Heat Mass Transf.* **2021**, *165*, 120665. [CrossRef]
- 25. Snegirev, A.Y. Statistical modeling of thermal radiation transfer in buoyant turbulent diffusion flames. *Combust. Flame* **2004**, 136, 51–71. [CrossRef]
- 26. Kabashnikov, V.P.; Kmit, G.I. Influence of Turbulent Fluctuations of Thermal Radiation. *J. Appl. Spectrosc.* **1979**, 31, 963–967. [CrossRef]
- 27. Kabashnikov, V.P.; Myasnikova, G.I. Thermal Radiation in Turbulent Flows—Temperature and Concentration Fluctuations. *Heat Transf.-Sov. Res.* **1985**, *17*, 116–125.
- 28. Li, G.; Modest, M.F. Application of composition PDF methods in the investigation of turbulence–radiation interactions. *J. Quant. Spectrosc. Radiat. Transf.* **2002**, *73*, 461–472. [CrossRef]
- 29. Li, G.; Modest, M.F. Importance of Turbulence–Radiation Interactions in Turbulent Diffusion Jet Flames. *ASME J. Heat Transf.* **2003**, *125*, 831–838. [CrossRef]
- 30. Wang, L.; Modest, M.F.; Haworth, D.C.; Turns, S.R. Modeling Nongray Soot and Gas-Phase Radiation in Luminous Turbulent Nonpremixed Jet Flames. *Combust. Theory Model.* **2005**, *9*, 479–498. [CrossRef]
- 31. Yang, X.; He, Z.; Dong, S.; Tan, H.P. Prediction of turbulence radiation interactions of CH<sub>4</sub>–H<sub>2</sub>/air turbulent flames at atmospheric and elevated pressures. *Int. J. Hydrogen Energy* **2018**, *43*, 15537–15550. [CrossRef]
- 32. Nmira, F.; Consalvi, J.L.; André, F. Pressure effects on radiative heat transfer in hydrogen/air turbulent diffusion flames. *J. Quant. Spectrosc. Radiat. Transf.* **2018**, 220, 172–179. [CrossRef]
- 33. Nmira, F.; Liu, Y.; Consalvi, J.L.; Andre, F.; Liu, F. Pressure effects on radiative heat transfer in sooting turbulent diffusion flames. J. Quant. Spectrosc. Radiat. Transf. 2020, 245, 106906. [CrossRef]

Energies **2023**, 16, 4250 34 of 40

34. Mehta, R.S.; Wang, A.; Modest, M.F.; Haworth, D.C. Modeling of a Turbulent Ethylene/Air Flame Using Hybrid Finite Volume/Monte Carlo Methods. *Comput. Therm. Sci.* **2009**, *1*, 37–53. [CrossRef]

- 35. Mehta, R.S.; Haworth, D.C.; Modest, M.F. Composition PDF/photon Monte Carlo Modeling of Moderately Sooting Turbulent Jet Flames. *Combust. Flame* **2010**, 157, 982–994. [CrossRef]
- 36. Mehta, R.S.; Modest, M.F.; Haworth, D.C. Radiation Characteristics and Turbulence–Radiation Interactions in Sooting Turbulent Jet Flames. *Combust. Theory Model.* **2010**, *14*, 105–124. [CrossRef]
- 37. Consalvi, J.L.; Nmira, F. Absorption turbulence–radiation interactions in sooting turbulent jet flames. *J. Quant. Spectrosc. Radiat. Transf.* **2017**, 201, 1–9. [CrossRef]
- 38. Nmira, F.; Consalvi, J.L. Local contributions of resolved and subgrid turbulence-radiation interaction in LES/presumed FDF modelling of large-scale methanol pool fires. *Int. J. Heat Mass Transf.* **2022**, *190*, 122746. [CrossRef]
- 39. Song, T.H.; Viskanta, R. Interaction of Radiation with Turbulence: Application to a Combustion System. *AIAA J. Thermophys. Heat Transf.* **1987**, *1*, 56–62. [CrossRef]
- 40. Consalvi, J.L. Influence of turbulence–radiation interactions in laboratory-scale methane pool fires. *Int. J. Therm. Sci.* **2012**, 60, 122–130. [CrossRef]
- 41. Cumber, P.S. Validation study of a turbulence radiation interaction model: Weak, intermediate and strong TRI in jet flames. *Int. J. Heat Mass Transf.* **2014**, *79*, 1034–1047. [CrossRef]
- 42. Cumber, P.S. Efficient Modeling of Turbulence-Radiation Interaction in Subsonic Hydrogen Jet Flames. *Numer. Heat Transf. Part B* **2013**, *63*, 85–114. [CrossRef]
- 43. Consalvi, J.L.; Demarco, R.; Fuentes, A. Modelling thermal radiation in buoyant turbulent diffusion flames. *Combust. Theory Model.* **2012**, *16*, 817–841. [CrossRef]
- 44. Cumber, P.S.; Onokpe, O. Turbulent radiation interaction in jet flames: Sensitivity to the PDF. *Int. J. Heat Mass Transf.* **2013**, 57, 250–264. [CrossRef]
- 45. Young, X.; He, Z.; Niu, Q.; Dong, S.; Tan, H. Numerical analysis of turbulence radiation interaction effect on radiative heat transfer in a swirling oxyfuel furnace. *Int. J. Heat Mass Transf.* **2019**, *141*, 1227–1237. [CrossRef]
- 46. Sivathanu, Y.R.; Kounalakis, M.E.; Faeth, G.M. Soot and Continuous Radiation Statistics of Luminous Turbulent Diffusion Flames. In Proceedings of the Twenty-Third Symposium (International) on Combustion, Orléans, France, 22–27 July 1990; The Combustion Institute: Pittsburgh, PA, USA, 1990; pp. 1543–1550.
- 47. Kounalakis, M.E.; Sivathanu, Y.R.; Faeth, G.M. Infrared Radiation Statistics of Nonluminous Turbulent Diffusion Flames. *ASME J. Heat Transf.* **1991**, *113*, 437–445. [CrossRef]
- 48. Fraga, G.C.; Coelho, P.J.; Petry, A.P.; França, F.H.R. Development and testing of a model for turbulence-radiation interaction effects on the radiative emission. *J. Quant. Spectrosc. Radiat. Transf.* **2020**, 245, 106852. [CrossRef]
- 49. Fraga, G.C.; Centeno, F.R.; Petry, A.P.; Coelho, P.J.; França, F.H.R. On the individual importance of temperature and concentration fluctuations in the turbulence-radiation interaction in pool fires. *Int. J. Heat Mass Transf.* **2019**, *136*, 1079–1089. [CrossRef]
- 50. Armengol, J.M.; Vicquelin, R.; Coussement, A.; Santos, R.G.; Gicquel, O. Study of turbulence-radiation interactions in a heated jet using direct numerical simulation coupled to a non-gray Monte-Carlo solver. *Int. J. Heat Mass Transf.* **2020**, *162*, 187–203. [CrossRef]
- 51. Nmira, F.; Burot, D.; Consalvi, J.L. Stochastic Eulerian field method for radiative heat transfer in a propane oxygen-enhanced turbulent diffusion flame. *Combust. Theory Model.* **2017**, 21, 62–78. [CrossRef]
- 52. Consalvi, J.L.; Nmira, F. Effects of soot absorption coefficient-Planck function correlation on radiative heat transfer in oxygenenriched propane turbulent diffusion flame. *J. Quant. Spectrosc. Radiat. Transf.* **2016**, 172, 50–57. [CrossRef]
- 53. Nmira, F.; Burot, D.; Consalvi, J.L. Soot emission radiation-turbulence interactions in diffusion jet flames. *Combust. Sci. Technol.* **2019**, *191*, 126–136. [CrossRef]
- 54. Chandy, A.J.; Glaze, D.J.; Frankel, S.H. A General Semicausal Stochastic Model for Turbulence/Radiation Interactions in Flames. ASME J. Heat Transf. 1997, 113, 509–516. [CrossRef]
- 55. Roger, M.; Silva, C.B.D.; Coelho, P.J. Analysis of the turbulence–radiation interactions for large eddy simulations of turbulent flows. *Int. J. Heat Mass Transf.* **2009**, 52, 2243–2254. [CrossRef]
- 56. Roger, M.; Coelho, P.J.; da Silva, C.B. The influence of the non-resolved scales of thermal radiation in large eddy simulation of turbulent flows: A fundamental study. *Int. J. Heat Mass Transf.* **2010**, *53*, 2897–2907. [CrossRef]
- 57. Gupta, A.; Haworth, D.C.; Modest, M.F. Turbulence–radiation interactions in large-eddy simulations of luminous and nonluminous nonpremixed flames. *Proc. Combust. Inst.* **2013**, *34*, 1281–1288. [CrossRef]
- 58. Gupta, A. Large-Eddy Simulation of Turbulent Flames with Radiation Heat Transfer. Ph.D. Thesis, The Pennsylvania State University, University Park, PA, USA, 2011.
- 59. Coelho, P.J. Approximate solutions of the filtered radiative transfer equation in large eddy simulations of turbulent reactive flows. *Combust. Flame* **2009**, *156*, 1099–1110. [CrossRef]
- 60. Consalvi, J.L.; Nmira, F.; Kong, W. On the modeling of the filtered radiative transfer equation in large eddy simulations of lab-scale sooting turbulent diffusion flames. *J. Quant. Spectrosc. Radiat. Transf.* **2018**, 221, 51–60. [CrossRef]
- 61. Roger, M.; Coelho, P.J.; da Silva, C.B. Relevance of the subgrid-scales for large eddy simulations of turbulence–radiation interactions in a turbulent plane jet. *J. Quant. Spectrosc. Radiat. Transf.* **2011**, *112*, 1250–1256. [CrossRef]

Energies **2023**, 16, 4250 35 of 40

62. Miranda, F.C.; Coelho, P.J.; di Mare, F.; Janicka, J. Study of turbulence-radiation interactions in large-eddy simulation of scaled Sandia flame D. *J. Quant. Spectrosc. Radiat. Transf.* **2019**, 228, 47–56. [CrossRef]

- 63. Fraga, G.C.; Miranda, F.C.; França, F.H.R.; Janicka, J.; Coelho, P.J. Assessment of a model for emission subgrid-scale turbulence-radiation interaction applied to a scaled Sandia flame DD. *J. Quant. Spectrosc. Radiat. Transf.* **2020**, 248, 106986. [CrossRef]
- 64. Poitou, D.; Amaya, J.; El Hafi, M.; Cuénot, B. Analysis of the interaction between turbulent combustion and thermal radiation using unsteady coupled LES/DOM simulations. *Combust. Flame* **2012**, *159*, 1605–1618. [CrossRef]
- 65. Deshmukh, K.V.; Haworth, D.C.; Modest, M.F. Direct Numerical Simulation of Turbulence–Radiation Interactions in a Statistically Homogeneous Nonpremixed Combustion System. *Proc. Combust. Inst.* **2007**, *31*, 1641–1648. [CrossRef]
- 66. Kang, S.H. Direct numerical simulation of the turbulent premixed flame propagation with radiation effects. *Int. J. Heat Mass Transf.* **2016**, *102*, 323–330. [CrossRef]
- 67. Rejeb, S.B.; Echekki, T. Thermal radiation modeling using the LES-ODT framework for turbulent combustion flows. *Int. J. Heat Mass Transf.* **2017**, *104*, 1300–1316. [CrossRef]
- 68. Silvestri, S.; Roekaerts, D.J.E.M.; Pecnik, R. Assessing turbulence-radiation interactions in turbulent flows of non-gray media. *J. Quant. Spectrosc. Radiat. Transf.* **2019**, 233, 134–148. [CrossRef]
- 69. Gordon, I.E.; Rothman, L.S.; Hargreaves, R.J.; Hashemi, R.; Karlovets, E.V.; Skinner, F.M.; Conway, E.K.; Hill, C.; Kochanov, R.V.; Tan, Y.; et al. The HITRAN2020 molecular spectroscopic database. *J. Quant. Spectrosc. Radiat. Transf.* **2022**, 277, 107949. [CrossRef]
- 70. Rothman, L.S.; Gordon, I.E.; Barber, R.J.; Dothe, H.; Gamache, R.R.; Goldman, A.; Perevalov, V.I.; Tashkun, S.A.; Tennyson, J. HITEMP, the high-temperature molecular spectroscopic database. *J. Quant. Spectrosc. Radiat. Transf.* **2010**, *111*, 2139–2150. [CrossRef]
- 71. Tashkun, S.A.; Perevalov, V.I.; Teffo, J.L.; Bykov, A.D.; Lavrentieva, N.N. CDSD-1000, the high-temperature carbon dioxide spectroscopic databank. *J. Quant. Spectrosc. Radiat. Transf.* **2003**, *82*, 165–196. [CrossRef]
- 72. Tashkun, S.A.; Perevalov, V.I. CDSD-4000: High-resolution, high-temperature carbon dioxide spectroscopic databank. *J. Quant. Spectrosc. Radiat. Transf.* **2011**, 112, 1403–1410. [CrossRef]
- 73. Fraga, G.C.; Bordbar, H.; Hostikka, S.; França, F.H.R. Benchmark Solutions of Three-Dimensional Radiative Transfer in Nongray Media Using Line-by-Line Integration. *ASME J. Heat Transf.* **2020**, *142*, 034510. [CrossRef]
- 74. Coelho, F.R.; Ziemniczak, A.; Roy, S.P.; França, F.H.R. A new line-by-line methodology based on the spectral contributions of the bands. *Int. J. Heat Mass Transf.* **2021**, *164*, 120423. [CrossRef]
- 75. Bond, T.C.; Bergstrom, R.W. Light Absorption by Carbonaceous Particles: An Investigative Review Light Absorption by Carbonaceous Particles: An Investigative Review. *Aerosol Sci. Technol.* **2007**, *40*, 27–67. [CrossRef]
- 76. Thomson, M.J. Modeling soot formation in flames and reactors: Recent progress and current challenges. *Proc. Combust. Inst.* 2022, *In Press.* [CrossRef]
- 77. Bond, T.C.; Doherty, S.J.; Fahey, D.W.; Forster, P.M.; Berntsen, T.; DeAngelo, B.J.; Flanner, M.G.; Ghan, S.; Kärcher, B.; Koch, D.; et al. Bounding the role of black carbon in the climate system: A scientific assessment. *J. Geophys. Res. Atmos.* **2013**, *118*, 5380—-5552. [CrossRef]
- 78. D'Alessio, A.; D'Anna, A.; Gambi, G.; Minutolo, P. The spectroscopic characterisation of UV absorbing nanoparticles in fuel rich soot forming flames. *J. Aerosol Sci.* **1998**, 29, 397–409. [CrossRef]
- 79. Michelsen, H.A. Probing soot formation, chemical and physical evolution, and oxidation: A review of in situ diagnostic techniques and needs. *Proc. Combust. Inst.* **2017**, *36*, 717–735. [CrossRef]
- 80. Kelesidis, G.A.; Pratsinis, S.E. Soot light absorption and refractive index during agglomeration and surface growth. *Proc. Combust. Inst.* **2019**, 37, 1177–1184. [CrossRef]
- 81. Michelsen, H.A.; Colket, M.B.; Bengtsson, P.E.; D'Anna, A.; Desgroux, P.; Haynes, B.S.; Miller, J.H.; Nathan, G.J.; Pitsch, H.; Wang, H. A review of terminology used to describe soot formation and evolution under combustion and pyrolytic conditions. *ACS Nano* 2020, *14*, 12470–12490. [CrossRef]
- 82. Stull, V.R.; Plass, G.N. Emissivity of Dispersed Carbon Particles. J. Opt. Soc. Am. 1960, 50, 121. [CrossRef]
- 83. Millikan, R.C. Optical Properties of Soot. J. Opt. Soc. Am. 1961, 51, 698–699. [CrossRef]
- 84. Dalzell, W.H.; Sarofim, A.F. Optical constants of soot and their application to heat-flux calculations. *ASME J. Heat Transf.* **1969**, 91, 100–104. [CrossRef]
- 85. Lee, S.; Tien, C. Optical constants of soot in hydrocarbon flames. Symp. (Int.) Combust. 1981, 18, 1159–1166. [CrossRef]
- 86. Charalampopoulos, T.; Chang, H. Effects of soot agglomeration on radiative transfer. *J. Quant. Spectrosc. Radiat. Transf.* **1991**, 46, 125–134. [CrossRef]
- 87. Minutolo, P.; Commodo, M.; DÁnna, A. Optical properties of incipient soot. Proc. Combust. Inst. 2022, In press. [CrossRef]
- 88. Liu, F.; Yon, J.; Fuentes, A.; Lobo, P.; Smallwood, G.J.; Corbin, J.C. Review of recent literature on the light absorption properties of black carbon: Refractive index, mass absorption cross section, and absorption function. *Aerosol Sci. Technol.* **2020**, *54*, 33–51. [CrossRef]
- 89. Kelesidis, G.A.; Crepaldi, P.; Allemann, M.; Duric, A.; Pratsinis, S.E. The mobility diameter of soot determines its angular light scattering distribution. *Combust. Flame* **2022**, 112476. [CrossRef]
- 90. Hostikka, S.; McGrattan, K. Numerical modeling of radiative heat transfer in water sprays. Fire Saf. J. 2006, 41, 76–86. [CrossRef]
- 91. Boulet, P.; Collin, A.; Parent, G. Heat transfer through a water spray curtain under the effect of a strong radiative source. *Fire Saf. J.* **2006**, *41*, 15–30. [CrossRef]

Energies **2023**, 16, 4250 36 of 40

92. Collin, A.; Boulet, P.; Lacroix, D.; Jeandel, G. On radiative transfer in water spray curtains using the discrete ordinates method. *J. Quant. Spectrosc. Radiat. Transf.* **2005**, 92, 85–110. [CrossRef]

- 93. Boulet, P.; Collin, A.; Consalvi, J.L. On the finite volume method and the discrete ordinates method regarding radiative heat transfer in acute forward anisotropic scattering media. *J. Quant. Spectrosc. Radiat. Transf.* **2007**, *104*, 460–473. [CrossRef]
- 94. Wu, B.; Zhao, X. Radiation characteristics of water droplets in a fire-inspired environment: A Monte Carlo ray tracing study. *J. Quant. Spectrosc. Radiat. Transf.* **2018**, 212, 97–111. [CrossRef]
- 95. Oluwole, O.O.; Gupta, A.; Wu, B.; Zhao, X.; Meredith, K.V.; Wang, Y. Nongray models for radiative absorption and anisotropic scattering by water droplets in fire CFD simulations. *Fire Saf. J.* **2021**, *120*, 103034. [CrossRef]
- 96. Anderson, M.R. Determination of Infrared Optical Constants for Single Component Hydrocarbon Fuels. Master's Thesis, University of Missouri-Rolla, Rolla, MO, USA, 2000.
- 97. Tuntomo, A. Transport Phenomena in a Small Particle with Internal Radiant Absorption. Ph.D. Thesis, University of California at Berkeley, Berkeley, CA, 1990.
- 98. Tuntomo, A.; Tien, C.L.; Park, S.H. Optical constants of liquid hydrocarbon fuels. *Combust. Sci. Technol.* 1992, 84, 133–140. [CrossRef]
- 99. Wang, C.C.; Tan, J.Y.; Jing, C.Y.; Liu, L.H. Temperature-dependent optical constants of liquid isopropanol, n-butanol, and n-decane. *Appl. Opt.* **2018**, *57*, 3003. [CrossRef] [PubMed]
- 100. Dombrovsky, L.A.; Sazhin, S.S.; Mikhalovsky, S.V.; Wood, R.; Heikal, M.R. Spectral Properties of Diesel Fuel Droplets. *Fuel* **2003**, 82, 15–22. [CrossRef]
- 101. Dombrovsky, L.A. Thermal Radiation From Nonisothermal Spherical Particles Of A Semitransparent Material. *Int. J. Heat Mass Transf.* **2000**, *43*, 1661–1672. [CrossRef]
- 102. Dombrovsky, L.A.; Baillis, D. *Thermal Radiation in Disperse Systems: An Engineering Approach*; Begell House: New York, NY, USA, 2010.
- 103. Dombrovsky, L.A. Spectral Model of Absorption and Scattering of Thermal Radiation by Diesel Fuel Droplets. *High Temp.* **2002**, 40, 242–248. [CrossRef]
- 104. Penner, S.S. Quantitative Molecular Spectroscopy and Gas Emissivities; Addison Wesley: Reading, MA, USA, 1960.
- 105. Paul, C.; Haworth, D.C.; Modest, M.F. A simplified CFD model for spectral radiative heat transfer in high-pressure hydrocarbonair combustion systems. *Proc. Combust. Inst.* **2019**, *37*, 4617–4624. [CrossRef]
- 106. Sikic, I.; Dembele, S.; Wen, J. Non-grey radiative heat transfer modelling in LES-CFD simulated methanol pool fires. *J. Quant. Spectrosc. Radiat. Transf.* **2019**, 234, 78–89. [CrossRef]
- 107. Edwards, D.K. Molecular Gas Band Radiation. In *Advances in Heat Transfer*; Academic Press: New York, NY, USA, 1976; Volume 12, pp. 115–193.
- 108. Grosshandler, W.L. *RADCAL: A Narrow-Band Model for Radiation Calculations in a Combustion Environment;* Technical Report NIST Technical Note 1402; National Institute of Standards and Technology: Gaithersburg, MD, USA, 1993.
- 109. Soufiani, A.; Taine, J. High temperature gas radiative property parameters of statistical narrow-band model for H<sub>2</sub>O, CO<sub>2</sub> and CO, and correlated-*k* model for H<sub>2</sub>O and CO<sub>2</sub>. *Int. J. Heat Mass Transf.* **1997**, 40, 987–991. [CrossRef]
- 110. Rivière, P.; Soufiani, A. Updated band model parameters for H<sub>2</sub>O, CO<sub>2</sub>, CH<sub>4</sub> and CO radiation at high temperature. *Int. J. Heat Mass Transf.* **2012**, *55*, 3349–3358. [CrossRef]
- 111. Fisher, A.; Rani, S. A narrow band model based on the absorption coefficient and its application to the calculation of radiative transfer in one-dimensional enclosures. *J. Quant. Spectrosc. Radiat. Transf.* **2022**, 277, 107989. [CrossRef]
- 112. Modest, M.F. The Weighted-Sum-of-Gray-Gases Model for Arbitrary Solution Methods in Radiative Transfer. *ASME J. Heat Transf.* 1991, 113, 650–656. [CrossRef]
- 113. Kangwanpongpan, T.; França, F.H.R.; da Silva, R.C.; Schneider, P.S.; Krautz, H.J. New correlations for the weighted-sum-of-gray-gases model in oxy-fuel conditions based on HITEMP 2010 database. *Int. J. Heat Mass Transf.* **2012**, *55*, 7419–7433. [CrossRef]
- 114. Dorigon, L.J.; Duciak, G.; Brittes, R.; Cassol, F.; Galarça, M.; França, F.H.R. WSGG correlations based on HITEMP2010 for computation of thermal radiation in non-isothermal, non-homogeneous H<sub>2</sub>O/CO<sub>2</sub> mixtures. *Int. J. Heat Mass Transf.* **2013**, 64, 863–873. [CrossRef]
- 115. Wang, B.; Xuan, Y. An improved WSGG model for exhaust gases of aero engines within broader ranges of temperature and pressure variations. *Int. J. Heat Mass Transf.* **2019**, *136*, 1299–1310. [CrossRef]
- 116. Bordbar, H.; Coelho, F.R.; Fraga, G.C.; França, F.H.R.; Hostikka, S. Pressure-dependent weighted-sum-of-gray-gases models for heterogeneous CO<sub>2</sub>-H<sub>2</sub>O mixtures at sub- and super-atmospheric pressure. *Int. J. Heat Mass Transf.* **2021**, *173*, 121207. [CrossRef]
- 117. Bordbar, M.H.; Wecel, G.; Hyppänen, T. A line by line based weighted sum of gray gases model for inhomogeneous CO<sub>2</sub>–H<sub>2</sub>O mixture in oxy-fired combustion. *Combust. Flame* **2014**, *161*, 2435–2445. [CrossRef]
- 118. He, Z.; Dong, C.; Liang, D.; Mao, J. A weighted-sum-of-gray soot-fractal-aggregates model for nongray heat radiation in the high temperature gas-soot mixture. *J. Quant. Spectrosc. Radiat. Transf.* **2021**, 260, 107431. [CrossRef]
- 119. Guo, J.; Shen, L.; He, X.; Liu, Z.; Im, H.G. Assessment of weighted-sum-of-gray-gases models for gas-soot mixture in jet diffusion flames. *Int. J. Heat Mass Transf.* **2021**, *181*, 121907. [CrossRef]

Energies **2023**, 16, 4250 37 of 40

120. da Fonseca, R.J.C.; Fraga, G.C.; Coelho, F.R.; França, F.H.R. A wide-band based weighted-sum-of-gray-gases model for participating media: Application to H<sub>2</sub>O–CO<sub>2</sub> mixtures with or without soot. *Int. J. Heat Mass Transf.* **2023**, 204, 123839. [CrossRef]

- 121. Cassol, F.; Brittes, R.; França, F.H.R.; Ezekoye, O.A. Application of the weighted-sum-of-gray-gases model for media composed of arbitrary concentrations of H<sub>2</sub>O, CO<sub>2</sub> and soot. *Int. J. Heat Mass Transf.* **2014**, *79*, 796–806. [CrossRef]
- 122. Selhorst, A.H.B.; Fraga, G.C.; Coelho, F.R.; Bordbar, H.; França, F.H.R. A Compact WSGG Formulation to Account for Inhomogeneity of H<sub>2</sub>O–CO<sub>2</sub> Mixtures in Combustion Systems. *ASME J. Heat Transf.* **2022**, 144, 071301. [CrossRef]
- 123. Young, X.; He, Z.; Dong, S.; Tan, H. Evaluation of the non-gray weighted sum of gray gases models for radiative heat transfer in realistic non-isothermal and non-homogeneous flames using decoupled and coupled calculations. *Int. J. Heat Mass Transf.* **2019**, 134, 226–236. [CrossRef]
- 124. Chen, Q.; Yuen, A.C.Y.; Chen, T.B.Y.; Cao, R.F.; Liu, H.; Yeoh, G.H. A Large-Eddy Simulation study on the effect of fuel configuration and pan distance towards chemical species for under-ventilated compartment fire scenario. *Int. J. Heat Mass Transf.* **2022**, *184*, 122306. [CrossRef]
- 125. Denison, M.K.; Webb, B.W. A Spectral Line Based Weighted-Sum-of-Gray-gases Model for Arbitrary RTE Solvers. *ASME J. Heat Transf.* 1993, 115, 1004–1012. [CrossRef]
- 126. Denison, M.K.; Webb, B.W. The Spectral-Line-Based Weighted-Sum-of-Gray-Gases Model in Nonisothermal Nonhomogeneous Media. *ASME J. Heat Transf.* 1995, 117, 359–365. [CrossRef]
- 127. Denison, M.K.; Webb, B.W. The Spectral-Line Weighted-Sum-of-Gray-Gases Model for H<sub>2</sub>O/CO<sub>2</sub> Mixtures. *ASME J. Heat Transf.* **1995**, 117, 788–792. [CrossRef]
- 128. Solovjov, V.P.; Webb, B.W. SLW Modeling of Radiative Transfer in Multicomponent Gas Mixtures. *J. Quant. Spectrosc. Radiat. Transf.* 2000, 65, 655–672. [CrossRef]
- 129. Solovjov, V.P.; Webb, B.W. An Efficient Method of Modeling Radiative Transfer in Multicomponent Gas Mixtures With Soot. *ASME J. Heat Transf.* **2001**, 123, 450–457. [CrossRef]
- 130. Solovjov, V.P.; André, F.; Lemonnier, D.; Webb, B.W. The rank correlated SLW model of gas radiation in non-uniform media. *J. Quant. Spectrosc. Radiat. Transf.* **2017**, 197, 26–44. [CrossRef]
- 131. Ozen, G.; Ates, G.; Selçuk, N.; Kulah, G. Assessment of SLW-1 model in the presence of gray and non-gray particles. *Int. J. Therm. Sci.* **2019**, *136*, 420–432. [CrossRef]
- 132. Yasar, M.; Ozen, G.; Selçuk, N.; Kulah, G. Performance of banded SLW-1 in presence of non-gray walls and particles in fluidized bed combustors. *J. Quant. Spectrosc. Radiat. Transf.* **2020**, 257, 107370. [CrossRef]
- 133. Sun, Y.; Ma, J.; Yu, Y.; Ye, B.; Gao, C. Efficient SLW models for water vapor and carbon dioxide based on neural network method. *J. Quant. Spectrosc. Radiat. Transf.* **2019**, 236, 106600. [CrossRef]
- 134. Galtier, M.; Woelffel, W.; André, F.; Solovjov, V.P.; Webb, B.W.; Roy, S. Assessment of narrow-band and full spectrum gas radiation methods in a real industrial glass furnace configuration. *Appl. Therm. Eng.* **2022**, *216*, 119020. [CrossRef]
- 135. Lacis, A.A.; Oinas, V. A Description of the Correlated-*K* Distrib. Method Model. Nongray Gaseous Absorption, Therm. Emiss. Mult. Scatt. Vertically Inhomogeneous Atmos. *J. Geophys. Res.* **1991**, *96*, 9027–9063. [CrossRef]
- 136. Modest, M.F.; Zhang, H. The Full-Spectrum Correlated-K Distrib. Therm. Radiat. Mol. Gas- Mixtures. *ASME J. Heat Transf.* **2002**, 124, 30–38. [CrossRef]
- 137. Mazumder, S.; Modest, M.F. Application of the Full Spectrum Correlated-K Distrib. Approach Model. Non-Gray Radiat. Combust. Gases. *Combust. Flame* **2002**, *129*, 416–438. [CrossRef]
- 138. Pal, G.; Modest, M.F. A narrow-band based multi-scale multi-group full-spectrum *K* Distrib. Method Radiat. Transf. Nonhomogeneous Gas- Mixture. *ASME J. Heat Transf.* **2010**, *132*, 023307. [CrossRef]
- 139. Pal, G.; Modest, M.F. K-Distrib. Methods Radiat. Calc. High Press. Combust. *AIAA J. Thermophys. Heat Transf.* **2013**, 27, 584–587. [CrossRef]
- 140. Clements, A.G.; Porter, R.; Pranzitelli, A.; Pourkashanian, M. Evaluation of FSK models for radiative heat transfer under oxyfuel conditions. *J. Quant. Spectrosc. Radiat. Transf.* **2015**, *151*, *67*–75. [CrossRef]
- 141. Cai, J.; Modest, M.F. Improved full-spectrum *k*-distribution implementation for inhomogeneous media using a narrow-band database. *J. Quant. Spectrosc. Radiat. Transf.* **2013**, *141*, 65–72. [CrossRef]
- 142. Liu, G.; Liu, Y.; Liu, F.; Consalvi, J.L. A grouping strategy for the multi-group full-spectrum K-distribution method in gas mixtures. *J. Quant. Spectrosc. Radiat. Transf.* **2019**, 236, 106575. [CrossRef]
- 143. Alinejad, F.; Bordbar, H.; Hostikka, S. Development of full spectrum correlated k-model for spectral radiation penetration within liquid fuels. *Int. J. Heat Mass Transf.* **2020**, *158*, 119990. [CrossRef]
- 144. Liu, G.; Liu, Y.; Liu, F.; Consalvi, J.L.; Xu, J. A nongray-wall emissivity model for the full-spectrum correlated k-distribution method based on uniform media assumption. *Int. J. Heat Mass Transf.* **2021**, 179, 121660. [CrossRef]
- 145. Liu, G.; Liu, Y.; Zhu, J.; Consalvi, J.L.; Liu, F. An Improved nongray-wall emissivity-absorptivity model for the Full-Spectrum Correlated K-distribution method. *Int. J. Heat Mass Transf.* **2022**, *188*, 122604. [CrossRef]
- 146. Zhang, H.; Modest, M.F. Multi-Group Full-Spectrum *k*-Distribution Database ForWater Vapor Mixtures in Radiative Transfer Calculations. *Int. J. Heat Mass Transf.* **2003**, *46*, 3593–3603. [CrossRef]
- 147. Wang, C.; He, B.; Modest, M.F. Full-spectrum correlated-k-distribution look-up table for radiative transfer in nonhomogeneous participating media with gas-particle mixtures. *Int. J. Heat Mass Transf.* **2019**, 137, 1053–1063. [CrossRef]

Energies **2023**, 16, 4250 38 of 40

148. Liu, Y.; Zhu, J.; Liu, G.; Liu, F.; Consalvi, J.L. Assessment of various Full-Spectrum Correlated K-distribution methods in radiative heat transfer in oxy-fuel sooting flames. *Int. J. Therm. Sci.* **2023**, *184*, 107919. [CrossRef]

- 149. Wang, C.; Modest, M.F.; Ren, T.; Cai, J.; He, B. Comparison and refinement of the various full-spectrum k-distribution and spectral line weighted-sum-of-gray-gases models for nonhomogeneous media. *J. Quant. Spectrosc. Radiat. Transf.* **2021**, 271, 107695. [CrossRef]
- 150. Zhou, Y.; Wang, C.; Ren, T.; Zhao, C. A machine learning based full-spectrum correlated k-distribution model for nonhomogeneous gas-soot mixtures. *J. Quant. Spectrosc. Radiat. Transf.* **2021**, 268, 107628. [CrossRef]
- 151. Smyth, K.C.; Shaddix, C.R. The elusive history of m = 1.57 0.56i for the refractive index of soot. *Combust. Flame* **1996**, 107, 314–320. [CrossRef]
- 152. Colsalvi, J.L.; Andre, F.; Coelho, F.R.; França, F.H.R.; Nmira, F.; Galtier, M.; Solovjov, V.; Webb, B.W. Assessment of engineering gas radiative property models in high pressure turbulent jet diffusion flames. *J. Quant. Spectrosc. Radiat. Transf.* **2020**, 253, 107169. [CrossRef]
- 153. Chu, H.; Gu, M.; Consalvi, J.L.; Liu, F.; Zhou, H. Effects of total pressure on non-grey gas radiation transfer in oxy-fuel combustion using the LBL, SNB, SNBCK, WSGG, and FSCK methods. *J. Quant. Spectrosc. Radiat. Transf.* **2016**, *172*, 24–35. [CrossRef]
- 154. Chu, H.; Consalvi, J.L.; Gu, M.; Liu, F. Calculations of radiative heat transfer in an axisymmetric jet diffusion flame at elevated pressures using different gas radiation models. *J. Quant. Spectrosc. Radiat. Transf.* **2017**, 197, 12–25. [CrossRef]
- 155. André, F. The ℓ-distribution method for modeling non-gray absorption in uniform and non-uniform gaseous media. *J. Quant. Spectrosc. Radiat. Transf.* **2016**, *179*, 19–32. [CrossRef]
- 156. Andre, F.; Coelho, F.R.; Consalvi, J.L.; Franca, F.H.R.; Galtier, M.; Nmira, F.; Solovjov, V.P.; Webb, B.W. Accuracy of Engineering Methods for Radiative Transfer in CO<sub>2</sub>-H<sub>2</sub>O Mixtures at High Temperature. In Proceedings of the 9th International Symposium on Radiative Transfer, RAD-19, Athens, Greece, 3–7 June 2019; Begellhouse: Danbury, CT, USA, 2019; pp. 407–414.
- 157. Modest, M.F.; Yang, J. Elliptic PDE formulation and boundary conditions of the spherical harmonics method of arbitrary order for general three-dimensional geometries. *J. Quant. Spectrosc. Radiat. Transf.* **2008**, 109, 1641–1666. [CrossRef]
- 158. Cai, J.; Lei, S.; Dasgupta, A.; Modest, M.F.; Haworth, D.C. Radiative heat transfer in high-pressure laminar hydrogen–air diffusion flames. *Combust. Theory Model.* **2014**, *18*, 607–626. [CrossRef]
- 159. Garten, B.; Hunger, F.; Messig, D.; Stelzner, B.; Trimis, D.; Hasse, C. Detailed radiation modeling of a partial-oxidation flame. *Int. J. Therm. Sci.* **2015**, *87*, 68–84. [CrossRef]
- 160. Pal, G.; Gupta, A.; Modest, M.F.; Haworth, D.C. Comparison of accuracy and computational expense of radiation models in simulation of nonpremixed turbulent jet flames. *Combust. Flame* **2015**, *162*, 2487–2495. [CrossRef]
- 161. Wang, L.; Haworth, D.C.; Turns, S.R.; Modest, M.F. Interactions among soot, thermal radiation, and NOx emissions in oxygenenriched turbulent nonpremixed flames: A CFD modeling study. *Combust. Flame* **2005**, *141*. 170–179. [CrossRef]
- 162. Wang, L.; Endrud, N.E.; Turns, S.R.; D'Agostini, M.D.; Slavejkov, A.G. A Study of the Influence of Oxygen Index on Soot, Radiation, and Emissions Characteristics of Turbulent Jet Flames. *Combust. Sci. Technol.* **2002**, *174*, 45–72. [CrossRef]
- 163. Ge, W.; David, C.; Modest, M.F.; Sankaran, R.; Roy, S.P. Comparison of Spherical Harmonics Method and Discrete Ordinates Method for Radiative Transfer in a Turbulent Jet Flame. *J. Quant. Spectrosc. Radiat. Transf.* **2023**, 296, 108459. [CrossRef]
- 164. Chui, E.H.; Raithby, G.D.; Hughes, P.M.J. Prediction of Radiative Transfer in Cylindrical Enclosures with the Finite Volume Method. *AIAA J. Thermophys. Heat Transf.* **1992**, *6*, 605–611. [CrossRef]
- 165. Chui, E.H.; Raithby, G.D. Computation of Radiant Heat Transfer on a Nonorthogonal Mesh Using the Finite-Volume Method. *Numer. Heat Transf. Part B* **1993**, 23, 269–288. [CrossRef]
- 166. Chai, J.C.; Lee, H.S.; Patankar, S.V. Finite Volume Method for Radiation Heat Transfer. *AIAA J. Thermophys. Heat Transf.* **1994**, *8*, 419–425. [CrossRef]
- 167. Chai, J.C.; Parthasarathy, G.; Lee, H.S.; Patankar, S.V. Finite Volume Method Radiative Heat Transfer Procedure for Irregular Geometries. *AIAA J. Thermophys. Heat Transf.* **1995**, *9*, 410–415. [CrossRef]
- 168. Coelho, P.J. Discrete ordinates and finite volume methods. Thermopedia 2011. [CrossRef]
- 169. Mathur, S.R.; Murthy, J.Y. Coupled Ordinates Method for Multigrid Acceleration of Radiation Calculations. *AIAA J. Thermophys. Heat Transf.* **1999**, *13*, 467–473. [CrossRef]
- 170. Mathur, S.R.; Murthy, J.Y. Acceleration of Anisotropic Scattering Computations Using Coupled Ordinates Method (COMET). *ASME J. Heat Transf.* **1999**, 123, 607–612. [CrossRef]
- 171. Fuentes, A.; Henriquez, R.; Nmira, F.; Liu, F.; Consalvi, J.L. Experimental and numerical study of the effects of the oxygen index on the radiation characteristics of laminar coflow diffusion flames. *Combust. Flame* **2013**, *160*, 786–795. [CrossRef]
- 172. Liu, F.; Consalvi, J.L.; Fuentes, A. Effects of water vapor addition to the air stream on soot formation and flame properties in a laminar coflow ethylene/air diffusion flame. *Combust. Flame* **2014**, *161*, 1724–1734. [CrossRef]
- 173. Demarco, R.; Nmira, F.; Consalvi, J.L. Influence of thermal radiation on soot production in laminar axisymmetric diffusion flames. *J. Quant. Spectrosc. Radiat. Transf.* **2013**, *120*, 52–69. [CrossRef]
- 174. Asllanaj, F.; Contassot-Vivier, S.; Botella, O.; França, F.H.R. Numerical solutions of radiative heat transfer in combustion systems using a parallel modified discrete ordinates method and several recent formulations of WSGG model. *J. Quant. Spectrosc. Radiat. Transf.* 2021, 274, 107863. [CrossRef]
- 175. Mazumder, S. *Numerical Methods for Partial Differential Equations: Finite Difference and Finite Volume Methods*; Academic Press: Cambridge, MA, USA, 2016.

Energies **2023**, 16, 4250 39 of 40

176. Yasar, M.S.; Selçuk, N.; Kulah, G. Performance and validation of a radiation model coupled with a transient bubbling fluidized bed combustion model. *Int. J. Therm. Sci.* **2022**, *176*, 107496. [CrossRef]

- 177. Modest, M.F. The Monte Carlo Method Applied to Gases with Spectral Line Structure. *Numer. Heat Transf. Part B* **1992**, 22, 273–284. [CrossRef]
- 178. Farmer, J.T.; Howell, J.R. Monte Carlo Prediction of Radiative Heat Transfer in Inhomogeneous, Anisotropic, Nongray Media. *AIAA J. Thermophys. Heat Transf.* **1994**, *8*, 133–139. [CrossRef]
- 179. Wang, L.; Yang, J.; Modest, M.F.; Haworth, D.C. Application of the Full-Spectrum k-Distribution Method to Photon Monte Carlo Solvers. *J. Quant. Spectrosc. Radiat. Transf.* **2007**, *104*, 297–304. [CrossRef]
- 180. Wang, A.; Modest, M.F. Spectral Monte Carlo Models for Nongray Radiation Analyses in Inhomogeneous Participating Media. *Int. J. Heat Mass Transf.* **2007**, *50*, 3877–3889. [CrossRef]
- 181. Ren, T.; Modest, M.F. Hybrid wavenumber selection scheme for line-by-line photon Monte Carlo simulations in high-temperature gases. *ASME J. Heat Transf.* **2013**, *135*, 084501. [CrossRef]
- 182. Marquez, R.; Modest, M.F.; Cai, J. Spectral Photon Monte Carlo with Energy Splitting Across Phases for Gas-Particle Mixtures. *ASME J. Heat Transf.* **2015**, 137, 121012. [CrossRef]
- 183. Roy, S.P.; Cai, J.; Modest, M.F. Development of a multiphase photon Monte Carlo method for spray combustion and its application in high-pressure conditions. *Int. J. Heat Mass Transf.* **2017**, *115 Pt A*, 453–466. [CrossRef]
- 184. Ren, T.; Modest, M.F.; Roy, S. Monte Carlo simulation for radiative transfer in a high-pressure industrial gas turbine combustion chamber. *J. Eng. Gas Turbines Power* **2018**, *140*, 051503. [CrossRef]
- 185. Rodrigues, P.; Gicquel, O.; Franzelli, B.; Darabiha, N.; Vicquelin, R. Analysis of radiative transfer in a turbulent sooting jet flame using a Monte Carlo method coupled to large eddy simulation. *J. Quant. Spectrosc. Radiat. Transf.* **2019**, 235, 187–203. [CrossRef]
- 186. Farmer, J.; Roy, S.P. A quasi-Monte Carlo solver for thermal radiation in participating media. *J. Quant. Spectrosc. Radiat. Transf.* **2020**, 242, 106753. [CrossRef]
- 187. Wu, B.; Zhao, X. Effects of radiation models on steady and flickering laminar non-premixed flames. *J. Quant. Spectrosc. Radiat. Transf.* **2020**, 253, 107103. [CrossRef]
- 188. Torres-Monclard, K.; Gicquel, O.; Vicquelin, R. A Quasi-Monte Carlo method to compute scattering effects in radiative heat transfer: Application to a sooted jet flame. *Int. J. Heat Mass Transf.* **2021**, *168*, 120915. [CrossRef]
- 189. Ren, T.; Modest, M.F. Line-by-line random-number database for photon Monte Carlo simulations of radiation in participating media. *ASME J. Heat Transf.* **2019**, 141, 0227019. [CrossRef]
- 190. Wang, C.; Modest, M.F.; He, B. Full-spectrum correlated-k-distribution look-up table for use with radiative Monte Carlo solvers. *Int. J. Heat Mass Transf.* **2019**, *131*, 167–175. [CrossRef]
- 191. Wu, B.; Roy, S.P.; Zhao, X.; Modest, M.F. Effect of multiphase radiation on coal combustion in a pulverized coal jet flame. *J. Quant. Spectrosc. Radiat. Transf.* **2017**, 197, 154–165. [CrossRef]
- 192. Kersch, A.; Morokoff, W.; Schuster, A. Radiative heat transfer with quasi-Monte Carlo methods. *Transp. Theory Stat. Phys.* **1994**, 23, 1001–1021. [CrossRef]
- 193. Mazumder, S.; Kersch, A. A Fast Monte Carlo Scheme for Thermal Radiation in Semiconductor Processing Applications. *Numer. Heat Transf. Part B* **2000**, *37*, 185–199.
- 194. Marston, A.J.; Daun, K.J.; Collins, M.R. Geometric Optimization of Radiant Enclosures Containing Specularly-Reflecting Surfaces through Quasi-Monte Carlo Simulation. *Numer. Heat Transf. Part A* **2011**, *59*, 81–97. [CrossRef]
- 195. Palluotto, L.; Dumont, N.; Rodrigues, P.; Gicquel, O.; Vicquelin, R. Assessment of randomized Quasi-Monte Carlo method efficiency in radiative heat transfer simulations. *J. Quant. Spectrosc. Radiat. Transf.* **2019**, 236, 106570. [CrossRef]
- 196. Modest, M.F. The Modified Differential Approximation for Radiative Transfer in General Three-Dimensional Media. *AIAA J. Thermophys. Heat Transf.* **1989**, *3*, 283–288. [CrossRef]
- 197. Ravishankar, M.; Mazumder, S.; Sankar, M. Application of the modified differential approximation for radiative transfer to arbitrary geometry. *J. Quant. Spectrosc. Radiat. Transf.* **2010**, *111*, 2052–2069. [CrossRef]
- 198. Sankar, M.; Mazumder, S. Solution of the Radiative Transfer Equation in Three-Dimensional Participating Media Using a Hybrid Discrete Ordinates-Spherical Harmonics Method. *ASME J. Heat Transf.* **2012**, 134, 112702. [CrossRef]
- 199. Yadav, R.; Kushari, A.; Verma, A.K.; Eswaran, V. Weighted Sum of Gray Gas Modeling for Nongray Radiation in Combusting Environment Using the Hybrid Solution Methodology. *Numer. Heat Transf. Part B* **2013**, *64*, 174–197. [CrossRef]
- 200. Sun, Y.; Zhang, X. Contributions of gray gases in SLW for non-gray radiation heat transfer and corresponding accuracies of FVM and P1 method. *Int. J. Heat Mass Transf.* **2018**, *121*, 819–831. [CrossRef]
- 201. Sun, Y.; Shen, H.; Zheng, S.; Jiang, L. A hybrid non-gray gas radiation heat transfer solver based on OpenFOAM. *J. Quant. Spectrosc. Radiat. Transf.* 2022, 281, 108105. [CrossRef]
- 202. Jajal, N.; Mazumder, S. Hybrid Solver for the Radiative Transport Equation in Nongray Combustion Gases. In Proceedings of the ASME International Mechanical Engineering Congress and Exposition, Columbus, OH, USA, 30 October–3 November 2022; Paper no. IMECE2022–94556; ASME: Columbus, OH, USA, 2022; Volume 86700, p. V008T11A022.
- 203. Jajal, N.; Mazumder, S. A Hybrid Solver for the Radiative Transfer Equation in Nongray Combustion Gases. *Comput. Therm. Sci.* **2023**, *in press*. [CrossRef]
- 204. Sun, H.F.; Sun, F.X.; Xia, X.L. A line-by-line hybrid unstructured finite volume/Monte Carlo method for radiation transfer in 3D non-gray medium. *J. Quant. Spectrosc. Radiat. Transf.* **2018**, 205, 135–146. [CrossRef]

Energies **2023**, 16, 4250 40 of 40

205. Dobbins, R.R.; Hall, R.J.; Cao, S.; Bennett, B.A.V.; Colket, M.B.; Smooke, M.D. Radiative Emission and Reabsorption in Laminar, Ethylene-Fueled Diffusion Flames Using the Discrete Ordinates Method. *Combust. Sci. Technol.* **2015**, *187*, 230–248. [CrossRef]

- 206. Orbegoso, E.M.; Figueira da Silva, L.F.; Serfaty, R. Comparative study of thermal radiation properties models in turbulent non-premixed sooting combustion. *Numer. Heat Transf. Part A* **2016**, *69*, 166–179. [CrossRef]
- 207. Mengüç, M.P.; Viskanta, R.; Ferguson, C. Multidimensional modeling of radiative heat transfer in Diesel engines. *SAE Trans.* **1985**, *94*, 728–745.
- 208. Kez, V.; Liu, F.; Consalvi, J.L.; Ströhle, J.; Epple, B. A comprehensive evaluation of different radiation models in a gas turbine combustor under conditions of oxy-fuel combustion with dry recycle. *J. Quant. Spectrosc. Radiat. Transf.* **2016**, 172, 121–133. [CrossRef]
- 209. Kez, V.; Consalvi, J.L.; Liu, F.; Ströhle, J.; Epple, B. Assessment of several gas radiation models for radiative heat transfer calculations in a three-dimensional oxy-fuel furnace under coal-fired conditions. *Int. J. Therm. Sci.* 2017, 120, 289–302. [CrossRef]
- 210. Paul, C.; Fernandez, S.F.; Haworth, D.C.; Roy, S.; Modest, M.F. A Detailed Modeling Study of Radiative Heat Transfer in a Heavy-Duty Diesel Engine. *Combust. Flame* **2019**, 200, 325–341. [CrossRef]
- 211. Porter, R.; Liu, F.; Pourkashanian, M.; Williams, A.; Smith, D. Evaluation of solution methods for radiative heat transfer in gaseous oxy-fuel combustion environments. *J. Quant. Spectrosc. Radiat. Transf.* **2010**, 111, 2084–2094. [CrossRef]
- 212. Tong, T.W.; Skocypec, R.D. Summary on Comparison of Radiative Heat Transfer Solutions for a Specified Problem. In Proceedings of the Developments in Radiative Heat Transfer, San Diego, CA, USA, 9–12 August 1992; ASME HTD: New York, NY, USA, 1992; Volume 203.
- 213. Iavarone, S.; Pascazio, L.; Sirignano, M.; De Candia, A.; Fierro, A.; de Arcangelis, L.; D'Anna, A. Molecular dynamics simulations of incipient carbonaceous nanoparticle formation at flame conditions. *Combust. Theory Model.* **2017**, 21, 49–61. [CrossRef]
- 214. Hou, D.; Pascazio, L.; Martin, J.; Zhou, Y.; Kraft, M.; You, X. On the reactive coagulation of incipient soot nanoparticles. *J. Aerosol Sci.* 2022, 159, 105866. [CrossRef]
- 215. Wang, Y.; Gu, M.; Wu, J.; Cao, L.; Lin, Y.; Huang, X. Formation of soot particles in methane and ethylene combustion: A reactive molecular dynamics study. *Int. J. Hydrogen Energy* **2021**, *46*, 36557–36568. [CrossRef]
- 216. Sharma, A.; Mukut, K.M.; Roy, S.P.; Goudeli, E. The coalescence of incipient soot clusters. Carbon 2021, 180, 215–225. [CrossRef]
- 217. Hu, H.; Li, Y.; Wei, Z.; Wang, Q. Parameter optimization for MSMGWB model used to calculate infrared remote sensing signals emitted by hot combustion gases of hydrocarbon fuel. *J. Quant. Spectrosc. Radiat. Transf.* **2020**, 249, 107003. [CrossRef]
- 218. Alinejad, F.; Bordbar, H.; Hostikka, S. Improving the modeling of spectral radiation penetration into the condensed materials with the separated full spectrum correlated-k method. *Int. J. Heat Mass Transf.* **2023**, *176*, 121448. [CrossRef]
- 219. Zhou, Y.; Wang, C.; Ren, T.; Zhao, C. A machine learning based efficient and compact full-spectrum correlated k-distribution model. *J. Quant. Spectrosc. Radiat. Transf.* **2020**, 254, 107199. [CrossRef]
- 220. Murthy, J.Y.; Mathur, S.R. Finite Volume Method for Radiative Heat Transfer Using Unstructured Meshes. *AIAA J. Thermophys. Heat Transf.* **1998**, 12, 313–321. [CrossRef]
- 221. Murthy, J.Y.; Mathur, S.R. Radiative heat transfer in axisymmetric geometries using an unstructured finite-volume method. *Numer. Heat Transf. Part B* **1998**, 33, 397–416. [CrossRef]
- 222. Liu, J.; Shang, H.M.; Chen, Y.S. Parallel simulation of radiative heat transfer using an unstructured finite-volume method. *Numer. Heat Transf. Part B* **1999**, *36*, 115–137.
- 223. Coelho, P.J. Application of high resolution NVD and TVD differencing schemes to the discrete ordinates method using unstructured grids. *J. Quant. Spectrosc. Radiat. Transf.* **2014**, *143*, 3–15. [CrossRef]
- 224. Ravishankar, M.; Mazumder, S.; Kumar, A. Finite-Volume Formulation and Solution of the *P*<sub>3</sub> Equations of Radiative Transfer on Unstructured Meshes. *ASME J. Heat Transf.* **2010**, *132*, 023402. [CrossRef]
- 225. Howell, J.R.; Daun, K.J. The Past and Future of the Monte Carlo Method in Thermal Radiation Transfer. *ASME J. Heat Transf.* **2021**, *143*, 100801. [CrossRef]
- 226. Ali, S.A.; Kollu, G.; Mazumder, S.; Sadayappan, P.; Mittal, A. Large-Scale Parallel Computation of the Phonon Boltzmann Transport Equation. *Int. J. Therm. Sci.* **2014**, *86*, 341–351. [CrossRef]
- 227. Fang, Q.; Yan, S. Graphics Processing Unit-Accelerated Mesh-Based Monte Carlo Photon Transport Simulations. *J. Biomed. Opt.* **2019**, 24, 115002. [CrossRef] [PubMed]
- 228. Fernando, M.; Neilsen, D.; Lim, H.; Hirschmann, E.; Sundar, H. Massively Parallel Simulations of Binary Black Hole Intermediate-Mass-Ratio Inspirals. *SIAM J. Sci. Comput.* **2019**, *41*, C97–C138. [CrossRef]
- 229. Heisler, E.; Deshmukh, A.; Mazumder, S.; Sadayappan, P.; Sundar, H. Multi-discretization domain specific language and code generation for differential equations. *J. Comput. Sci.* 2023, *68*, 101981. [CrossRef]

**Disclaimer/Publisher's Note:** The statements, opinions and data contained in all publications are solely those of the individual author(s) and contributor(s) and not of MDPI and/or the editor(s). MDPI and/or the editor(s) disclaim responsibility for any injury to people or property resulting from any ideas, methods, instructions or products referred to in the content.